COOPERATIVE BEHAVIOR IN NETWORKS OF COUPLED OSCILLATORS

A Dissertation

Presented to the Faculty of the Graduate School

of Cornell University

in Partial Fulfillment of the Requirements for the Degree of

Doctor of Philosophy

by

Erik Andreas Martens

May 2009

COOPERATIVE BEHAVIOR IN NETWORKS OF COUPLED OSCILLATORS

Erik Andreas Martens, Ph.D.

Cornell University 2009

This thesis comprises three problems related to the dynamics of coupled phase oscillators, described by variants of the Kuramoto model. Kuramoto originally made strong assumptions to simplify the analysis of the oscillator behavior: the phases obey a sinusoidal response curve, their natural frequencies are unimodally distributed, and the oscillators are globally coupled, i.e. all oscillators are coupled with equal strength. Investigating three problems we study what behavior may emerge as we relax the last two of these assumptions. In the first problem, we study the impact of replacing the unimodal with a bimodal frequency distribution on the oscillator dynamics. Based on a recent breakthrough in the field, we are able to determine the complete stability diagram, and determine all types of cooperative behavior that may occur. In the next two problems we break with the assumption of global coupling; a similar simplification that is frequently used is to consider the limit of local, i.e. nearest neighbor coupling. We investigate what types of new behavior emerge in the intermediate regime that we call nonlocal coupling, and study under which conditions it persists. For nonlocal coupling, a new kind of state has been observed, where synchronized and desynchronized oscillators coexist side by side in a stable fashion. This state is referred to as a chimera state. In the second problem we discuss a triangular network of oscillator populations with nonlocal coupling. For this network topology, we discover that bistable chimera attractors are possible. For the third problem, we study a generalization of this system, and break the ro-

tational symmetry inherent to the triangle by introducing an additional parameter. This parameter allows us to change the topology of the network continuously, such that the network attains a more chain-like character; this enables us to study the effect of network topology on the existence of chimera attractors.

BIOGRAPHICAL SKETCH

Erik Andreas Martens was born in Zürich, Switzerland on May 17, 1976. He attended the Kantonsschule Rychenberg (Gymnasium) in Winterthur (Switzerland), and attended the ETH Zürich (Swiss Federal Institute of Technology) (Switzerland), for his undergraduate studies, from where he earned his Master's degree in physics in 2004.

Til Mor og Far

ACKNOWLEDGEMENTS

I would like to express my deep gratitude to my mother and my father, my sister and my grandparents who either made much of my education possible or contributed significantly to it, for their love and support during many years.

Furthermore, without specific order on my mind, I would like to thank all of my friends who all have been helpful on my way to graduation in one or the other way; many people may go unmentioned who have not been of less importance to me. Hrusha for her love and support; Josh Bongard for his great friendship (and i...); Michael Moorehead for being a great fellow, his sense of humor and excelling sarcasm in moments of despair emerging in situations one really wouldn't want to be in, Sanjay Dharmavaram for being the coolest office mate I can imagine as well as his love for music, culture and Fruit Loops; Bo Pedersen for keeping my Danish humor alive and his seemingly endless source of ideas (or, to just have found a more creative way to procrastinate); Michael Wojnowicz for witty and cheerful remarks at all times; Anders Andersen for his friendship and advice, Gael Pressoir for teaching the break in between the work; Patrick Rameau for his friendship and his marvellous acting performances on the stages of Cornell's theater; Eric "Hi Erik" Gilbertson; Don Rohel for being a terrific landlord, and of course, Lyman Proaper for representing the most impressive inspiration about being a human at his 'mere' 92 years. Also I am grateful to the origin on the Ithacan Cartesian grid map system which has provided me with lots of fun.

Last but not least, I would like to express my special thanks to my advisors: Steve Strogatz, who taught me many inspiring and valuable lessons, which I many times think are applicable even beyond the scientist's paper and pencil world. I would also like to thank my committee members Richard Rand and

Paul Steen for their valuable teachings in class, for useful comments and to be very helpful at any time. A special tribute goes as well to Tomas Bohr for his mentorship, teaching, and conveying inspiration to do science, and of course, cheerful singing in the hallway.

TABLE OF CONTENTS

LIST OF FIGURES

PREFACE

The work presented in this thesis concerns three problems regarding the dynamics of coupled oscillators. Oscillating units appear in many areas of nature. Most often, oscillators are connected to one another in a complicated network, such that the dynamics of each individual unit also influences the motion of the other units. A phenomenon that all these types of coupled oscillator systems share is collective synchronization in which a network of oscillators lock to a common frequency, despite their difference in natural frequencies. Examples in biology include cardiac pacemaker cells, circadian pacemaker cells in the brain, metabolic synchrony in yeast cell suspensions and the synchronization of the flashing of fireflies. In physics we find examples in coupled arrays of lasers, microwave oscillators and superconducting Josephson junctions.

The question of which mechanisms underlie this type of cooperative behavior in coupled oscillator arrays was already posed by Norbert Wiener in the early sixties, and was later investigated by Arthur Winfree. One of the problems one faces while studying coupled oscillators is that the circumstances in which coupled oscillators appear in nature are not very uniform: for example, oscillators may have different natural frequencies; the units may even be heterogeneous in other, more general ways; the strength with which one oscillator couples to the motion of another may vary across the network; real physical systems are subject to thermal noise; and so on. Therefore, it was not until Kuramoto imposed strong assumptions on their nature that significant progress was made on the mathematical side of this complex problem. Based on his assumptions, Kuramoto developed a model that would enable him - using some very clever arguments - to explain the phenomenon of collective synchroniza-

tion. His model turned indeed out to be so successful that today, many variations of his original model are studied.

An important constraint Kuramoto imposed on the oscillators was to only let the oscillators be coupled weakly to one another. In this limit, the amplitude variations of the oscillations become negligible and so the problem reduces to a study of phase dynamics only. Despite this simplification, the resulting model is still quite general and the problem very hard to analyze. Therefore Kuramoto restricted the problem further by demanding the system behave as follows: the oscillators are globally coupled, i.e., all oscillators couple with equal strength; the dynamics of the phases are governed by a sinusoidal response curve; and finally, the natural frequencies of the oscillators are distributed unimodally in a uniform fashion. These assumptions are approximately true for at least some of the systems observed in nature.

The underlying idea pursued in this thesis is to investigate the behavior of coupled oscillators that emerges as we relax two of the assumptions in Kuramoto's original model, explained in what follows. Typically, the case of a unimodal frequency distribution is considered - but what happens if the distribution is *multimodal*? Chapter 1 addresses this generic case by extending the problem to the case of a *bimodal distribution*, which has been a longstanding problem in literature. Preliminary answers to what behavior might arise in this case were already given by Kuramoto [19], who originally posed this problem; however, the basis for his answers was intuitive in nature and would only partially predict the correct behavior. Later, Crawford [10] accomplished an impressive mathematical analysis of the problem, based on a center manifold reduction; this approach allowed him to obtain results for the weakly nonlinear

behavior in the neighborhood of the incoherent state, i.e. where the oscillators do not synchronize at all. In Chapter 1, we show that the long-term dynamics evolves to one of three states: *incoherence*, where all oscillators are desynchronized; *partial synchrony*, where a macroscopic group of phase-locked oscillators coesists with a sea of desynchronized ones; and a *standing wave* state, where two counter-rotating groups of phase-locked oscillators emerge. In addition, the complete stability diagram associated with this system is established.

In Chapters 2 and 3, we turn our attention to another question. One of Kuramoto's assumptions was that oscillators couple globally to one another, i.e. with equal strength. A different simplification often used in the literature assumes local coupling, i.e., nearest neighbor coupling. But what type of behavior emerges in the intermediate case, when we instead impose a *nonlocal* coupling that attenuates depending on the distance of the oscillators in a network? Such systems were recently studied by Kuramoto *et al.* [6, 20, 21]. Introducing this spatial character to the problem, they surprisingly found a state, where the oscillators split up into two continuous groups: one synchronized in phase and the other evolving in an entirely incoherent, i.e. desynchronized, fashion. Unfortunately, little was known about parameter regions allowing for these so called *chimera states*, or how they emerge. Much of the research presented in these chapters is inspired by these types of questions. A first study yielding some answers was done for a continuum of oscillators on a ring by Abrams *et al.* [2, 3]. The existence of chimera states on the ring naturally leads to the question whether chimerae could possibly appear on more physical domains such as the line. The analysis of this problem represents a challenge for a continuum of oscillators for a general topology, and therefore, discretization of space would lead to a more tractable problem. A system of three populations constitutes the

smallest network that can be connected in qualitatively different ways: a *triangle* (ring-like) and a *chain* (line-like). By introduction of an additional parameter we can break the rotational invariance of the triangle and 'tune' the network to behave more like a chain or a triangle. Two interesting findings were made on this journey: in Chapter 2, we discuss the emergence of bistable chimera states - unseen previously - on a purely triangular network. In Chapter 3, we break the triangular symmetry and discover that chimera states may exist on the chain-like network, with some restrictions.

Each of the three Chapters is presented in the form of a journal article that either has been published or is intended for publication in near future. The contents of Chapter 1 have already appeared in Phys. Rev. Lett. E [27].

CHAPTER 1

EXACT RESULTS FOR THE KURAMOTO PROBLEM WITH BIMODAL FREQUENCY DISTRIBUTION

* *This chapter is a reproduction of the same titled article by the authors E. A. Martens, E. Barreto, S. H. Strogatz, E. Ott, P. So, and T. M. Antonsen in Physical Review E* **79**, *026204 in 2009.*

1.1 Abstract

We analyze a large system of globally coupled phase oscillators whose natural frequencies are bimodally distributed. The dynamics of this system has been the subject of longstanding interest. In 1984 Kuramoto proposed several conjectures about its behavior; ten years later, Crawford obtained the first analytical results by means of a local center manifold calculation. Nevertheless, many questions have remained open, especially about the possibility of global bifurcations. Here we derive the system's stability diagram for the special case where the bimodal distribution consists of two equally weighted Lorentzians. Using an ansatz recently discovered by Ott and Antonsen, we show that in this case the infinite-dimensional problem reduces exactly to a flow in four dimensions. Depending on the parameters and initial conditions, the long-term dynamics evolves to one of three states: incoherence, where all the oscillators are desynchronized; partial synchrony, where a macroscopic group of phase-locked oscillators coexists with a sea of desynchronized ones; and a standing wave state, where two counter-rotating groups of phase-locked oscillators emerge. Analytical results are presented for the bifurcation boundaries between these states. Similar results are also obtained for the case in which the bimodal distribution is given by the sum of two Gaussians.

1.2 Introduction

1.2.1 Background

Large systems consisting of many coupled oscillatory units occur in a wide variety of situations [50, 17, 49]. Thus the study of the behaviors that such systems exhibit has been an active and continuing area of research. An important early contribution in this field was the introduction in 1975 by Kuramoto [18, 19] of a simple model which illustrates striking features of such systems. Kuramoto employed two key simplifications in arriving at his model: (i) the coupling between units was chosen to be homogeneous and all-to-all (i.e., 'global'), so that each oscillator would have an equal effect on all other oscillators; and (ii) the oscillator states were solely described by a phase angle $\theta(t)$, so that their uncoupled dynamics obeyed the simple equation $d\theta_i/dt = \omega_i$, where ω_i is the intrinsic natural frequency of oscillator i, $N \gg 1$ is the number of oscillators, and $i = 1, 2, \ldots, N$. The natural frequencies ω_i are, in general, different for each oscillator and are assumed to be drawn from some prescribed distribution function $g(\omega)$.

Much of the research on the Kuramoto model has focused on the case where $g(\omega)$ is unimodal (for reviews of this literature, see [44, 37, 4]). Specifically, g is usually assumed to be symmetric about a maximum at frequency $\omega = \omega_0$ and to decrease monotonically and continuously to zero as $|\omega - \omega_0|$ increases. In that case, it was found that as the coupling strength K between the oscillators increases from zero in the large-N limit, there is a continuous transition at a critical coupling strength $K_c = 2/(\pi g(\omega_0))$. For K below K_c, the average macroscopic, time-asymptotic behavior of the system is such that the oscillators in the system behave incoherently with respect to each other, and an order parame-

ter (defined in Sec. 1.3) is correspondingly zero. As K increases past K_c, the oscillators begin to influence each other in such a way that there is collective global organization in the phases of the oscillators, and the time-asymptotic order parameter assumes a non-zero constant value that increases continuously for $K > K_c$ [19, 44, 37, 4, 45].

It is natural to ask how these results change if other forms of $g(\omega)$ are considered. In this paper we will address this question for what is perhaps the simplest choice of a non-unimodal frequency distribution: we consider a distribution $g(\omega)$ that has two peaks [5, 35] and is the sum of two identical unimodal distributions $\hat{g}$, such that $g(\omega) = \frac{1}{2}[\hat{g}(\bar{\omega}-\omega_0)+\hat{g}(\bar{\omega}+\omega_0)]$. We find that this modification to the original problem introduces qualitatively new behaviors. As might be expected, this problem has been previously addressed [19, 10]. However, due to its difficulty, the problem was not fully solved, and, as we shall show, notable features of the behavior were missed.

1.2.2 Reduction method

The development that makes our analysis possible is the recent paper of Ott and Antonsen [38]. Using the method proposed in Ref. [38] we reduce the original problem formulation from an integro-partial-differential equation [44, 37, 45] for the oscillator distribution function (a function of ω, θ and t) to a system of just a few ordinary differential equations (ODEs). Furthermore, we analyze the reduced ODE system to obtain its attractors and the bifurcations they experience with variation of system parameters.

The reduced ODE system, however, represents a special restricted class of

all the possible solutions of the original full system [38]. Thus a concern is that the reduced system might miss some of the actual system behavior. In order to check this, we have done numerical solutions of the full system. The result is that, in all cases tested, the time-asymptotic attracting behavior of the full system and the observed attractor bifurcations are all contained in, and are quantitatively described by, our ODE formulation. Indeed a similar result applies for the application of the method of Ref. [38] to the original Kuramoto model with unimodally distributed frequencies [18, 19] and to the problem of the forced Kuramoto model with periodic drive [40, 9].

On the other hand, the reduction method has not been mathematically proven to capture all the attractors, for any of the systems to which it has been applied [38, 40, 9]. Throughout this paper we operate under the assumption (based on our numerical evidence) that the reduction method is reliable for the bimodal Kuramoto model. But we caution the reader that in general the situation is likely to be subtle and system-dependent; see Sec. 1.7.4 for further discussion of the scope and limits of the reduction method.

1.2.3 Outline of the paper

The organization of this paper is as follows. In Sec. 1.3 we formulate the problem and reduce it to the above-mentioned ODE description for the case where $g(\omega)$ is a sum of Cauchy-Lorentz distributions.

Sec. 1.4 provides an analysis of the ODE system. The main results of Sec. 1.4 are a delineation of the different types of attractors that can exist, the regions of parameter space that they occupy (including the possibility of bistability and

hysteresis), and the types of bifurcations that the attractors undergo.

In Sec. 1.5, we establish that the attractors of the ODEs obtained in Section 1.4 under certain symmetry assumptions are attractors of the full ODE system. In Section 1.6, we confirm that these attractors and bifurcations are also present in the original system. In addition, we investigate the case where $g(\omega)$ is a sum of Gaussians, rather than Cauchy-Lorentz distributions. We find that the attractors and bifurcations in the Lorentzian case and in the Gaussian case are of the same types and that parameter space maps of the different behaviors are qualitatively similar for the two distributions.

Finally, in Sec. 1.7 we compare our results to the earlier work of Kuramoto [19] and Crawford [10]. Then we discuss the scope and limits of the reduction method used here, and offer suggestions for future research.

1.3 Governing Equations

1.3.1 Problem definition

We study the Kuramoto problem of N oscillators with natural frequencies ω_i,

$$\frac{d\theta_i(t)}{dt} = \omega_i + \frac{K}{N}\sum_{j=1}^{N}\sin\Big(\theta_j(t) - \theta_i(t)\Big), \tag{1.1}$$

where θ_i are the phases of each individual oscillator and K is the coupling strength. We study this system in the limit $N \to \infty$ for the case in which the distribution of natural frequencies is given by the sum of two Lorentzian distributions:

$$g(\omega) = \frac{\Delta}{2\pi}\left(\frac{1}{(\omega-\omega_0)^2+\Delta^2} + \frac{1}{(\omega+\omega_0)^2+\Delta^2}\right). \tag{1.2}$$

Here Δ is the width parameter (half-width at half-maximum) of each Lorentzian and $\pm\omega_0$ are their center frequencies, as displayed in Fig. 1.1. A more physically relevant interpretation of ω_0 is as the *detuning* in the system (proportional to the separation between the two center frequencies). Note that we have written the

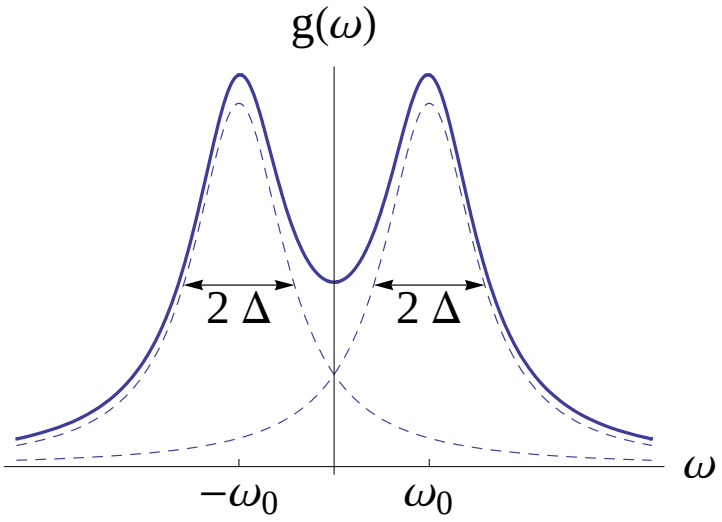

Figure 1.1: Bimodal distribution of natural frequencies, $g(\omega)$, consisting of the sum of two Lorentzians.

distribution $g(\omega)$ so that it is symmetric about zero; this can be achieved without loss of generality by going into a suitable rotating frame.

Another point to observe is that $g(\omega)$ is bimodal if and only if the peaks are sufficiently far apart compared to their widths. Specifically, one needs $\omega_0 > \Delta/\sqrt{3}$. Otherwise the distribution is unimodal and the classical results of [18, 19, 44, 37] would still apply.

1.3.2 Derivation

In the limit where $N \to \infty$, Eq. (1.1) can be written in a continuous formulation [19, 44, 37] in terms of a probability density $f(\theta, \omega, t)$. Here f is defined such that at time t, the fraction of oscillators with phases between θ and $\theta + d\theta$ and natural frequencies between ω and $\omega + d\omega$ is given by $f(\theta, \omega, t)\, d\theta\, d\omega$. Thus

$$\int_{-\infty}^{\infty} \int_{0}^{2\pi} f(\theta, \omega, t)\, d\theta\, d\omega = 1 \tag{1.3}$$

and

$$\int_{0}^{2\pi} f(\theta, \omega, t)\, d\theta = g(\omega), \tag{1.4}$$

by definition of $g(\omega)$.

The evolution of f is given by the continuity equation describing the conservation of oscillators:

$$\frac{\partial f}{\partial t} + \frac{\partial}{\partial \theta}(fv) = 0, \tag{1.5}$$

where $v(\theta, \omega, t)$ is the angular velocity of the oscillators. From Eq. (1.1), we have

$$v(\theta, \omega, t) = \omega + K \int_{0}^{2\pi} f(\theta', \omega, t) \sin(\theta' - \theta) d\theta'. \tag{1.6}$$

Following Kuramoto, we define a complex order parameter

$$z(t) = \int_{-\infty}^{\infty} \int_{0}^{2\pi} e^{i\theta} f(\theta, \omega, t)\, d\theta\, d\omega \tag{1.7}$$

whose magnitude $|z(t)| \leq 1$ characterizes the degree to which the oscillators are bunched in phase, and $\arg(z)$ describes the average phase angle of the oscillators. Expressing the velocity (1.6) in terms of z we obtain

$$v(\theta, \omega, t) = \omega + K \operatorname{Im}[z e^{-i\theta}] \tag{1.8}$$

$$= \omega + \frac{K}{2i}(z e^{-i\theta} - z^* e^{i\theta}), \tag{1.9}$$

where the * denotes complex conjugate.

Following Ott and Antonsen [38], we now restrict attention to a special class of density functions. By substituting a Fourier series of the form

$$f(\theta,\omega,t) = \frac{g(\omega)}{2\pi}\left[1 + \sum_{n=1}^{\infty}\left(f_n(\omega,t)e^{in\theta} + \text{c.c.}\right)\right], \tag{1.10}$$

where 'c.c' stands for the complex conjugate of the preceeding term, and imposing the ansatz that

$$f_n(\omega,t) = \alpha(\omega,t)^n, \tag{1.11}$$

we obtain

$$\frac{\partial\alpha}{\partial t} + \frac{K}{2}(z\alpha^2 - z^*) + i\omega\alpha = 0, \tag{1.12}$$

where

$$z^* = \int_{-\infty}^{\infty}\alpha(t,\omega)g(\omega)d\omega. \tag{1.13}$$

We now consider solutions of (1.12) and (1.13) for initial conditions $\alpha(\omega,0)$ that satisfy the following additional conditions: (i) $|\alpha(\omega,t)| \leq 1$; (ii) $\alpha(\omega,0)$ is analytically continuable into the lower half plane $\text{Im}(\omega) < 0$; and (iii) $|\alpha(\omega,t)| \to 0$ as $\text{Im}(\omega) \to -\infty$. If these conditions are satisfied for $\alpha(\omega,0)$, then, as shown in [38], they continue to be satisfied by $\alpha(\omega,t)$ as it evolves under Eqs. (1.12) and (1.13). Expanding $g(\omega)$ in partial fractions as

$$g(\omega) = \frac{1}{4\pi i}\left[\frac{1}{(\omega-\omega_0)-i\Delta} - \frac{1}{(\omega-\omega_0)+i\Delta} + \frac{1}{(\omega+\omega_0)-i\Delta} - \frac{1}{(\omega+\omega_0)+i\Delta}\right],$$

we find it has four simple poles at $\omega = \pm\omega_0 \pm i\Delta$. Evaluating (1.13) by deforming the integration path from the real ω-axis to $\text{Im}(\omega) \to -\infty$, the order parameter becomes

$$z(t) = \frac{1}{2}\left(z_1(t) + z_2(t)\right), \tag{1.14}$$

where

$$z_{1,2}(t) \;=\; \alpha^*(\pm\omega_0 - i\Delta, t). \tag{1.15}$$

Substitution of this expression into (1.12) yields two coupled complex ODEs, describing the evolution of two 'sub'-order parameters,

$$\begin{aligned} \dot{z}_1 \;&=\; -(\Delta + i\omega_0)z_1 \\ &\quad + \frac{K}{4}\left[z_1 + z_2 - (z_1^* + z_2^*)z_1^2\right] \end{aligned} \tag{1.16}$$

$$\begin{aligned} \dot{z}_2 \;&=\; -(\Delta - i\omega_0)z_2 \\ &\quad + \frac{K}{4}\left[z_1 + z_2 - (z_1^* + z_2^*)z_2^2\right], \end{aligned} \tag{1.17}$$

where we use dots to represent the time derivative from now on. (This system agrees with the results of [38] for the case of two equal groups of oscillators with uniform coupling strength and average frequencies ω_0 and $-\omega_0$.)

1.3.3 Reductions of the system

The system derived so far is four-dimensional. If we introduce polar coordinates $z_j = \rho_j e^{i\phi_j}$ and define the phase difference $\psi = \phi_2 - \phi_1$, the dimensionality can be reduced to three:

$$\dot{\rho}_1 \;=\; -\Delta\rho_1 + \frac{K}{4}(1-\rho_1^2)(\rho_1 + \rho_2\cos\psi) \tag{1.18}$$

$$\dot{\rho}_2 \;=\; -\Delta\rho_2 + \frac{K}{4}(1-\rho_2^2)(\rho_1\cos\psi + \rho_2) \tag{1.19}$$

$$\dot{\psi} \;=\; 2\omega_0 - \frac{K}{4}\,\frac{\rho_1^2 + \rho_2^2 + 2\rho_1^2\rho_2^2}{\rho_1\rho_2}\sin\psi. \tag{1.20}$$

To facilitate our analysis, we now look for solutions of Eqs. (1.18-1.20) that satisfy the symmetry condition

$$\rho_1(t) = \rho_2(t) \quad \equiv \quad \rho(t). \tag{1.21}$$

In Sec. 1.5 we will verify that these symmetric solutions are stable to perturbations away from the symmetry manifold and that the attractors of Eqs. (1.16, 1.17) lie within this manifold.

Our analysis of the problem thus reduces to a study in the phase plane:

$$\dot{\rho} = \frac{K}{4}\rho\left(1 - \frac{4\Delta}{K} - \rho^2 + (1-\rho^2)\cos\psi\right) \tag{1.22}$$

$$\dot{\psi} = 2\omega_0 - \frac{K}{2}(1+\rho^2)\sin\psi. \tag{1.23}$$

1.4 Bifurcation Analysis

Figure 1.2 summarizes the results of our analysis of Eqs. (1.22, 1.23). We find that three types of attractors occur: the well-known incoherent and partially synchronized states [18, 19, 44, 37, 4] corresponding to fixed points of (1.22, 1.23), as well as a standing wave state [10] corresponding to limit-cycle solutions. In addition, we will show that the transitions between these states are mediated by transcritical, saddle-node, Hopf, and homoclinic bifurcations, as well as by three points of higher codimension.

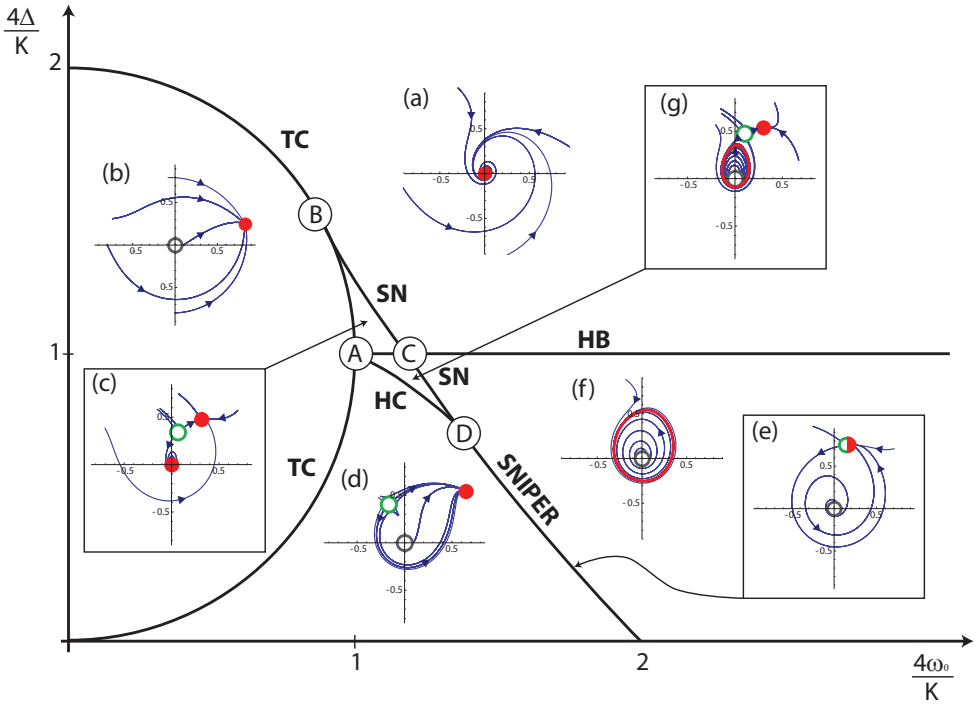

Figure 1.2: Bifurcation diagram for the Kuramoto system with a bimodal frequency distribution consisting of two equally weighted Lorentzians. The various bifurcation curves are denoted as follows: TC=transcritical, SN=saddle-node, HB=(degenerate) Hopf, HC=homoclinic, and SNIPER=Saddle-node-infinite-period. The insets, labeled (a)-(g), show (q, ψ) phase portraits (where $q = \rho^2$) in polar coordinates corresponding to the regions where the insets are located (see arrows for the boxed insets). Solid (red) dots and loops denote stable fixed point and limit cycles, respectively; open dots are saddle (green) or repelling (gray) fixed points. All parameters refer to their original (unscaled) versions.

1.4.1 Scaling

To ease the notation we begin by scaling Eqs. (1.22, 1.23). If we define $q = \rho^2$ and non-dimensionalize the parameters and time such that

$$\tilde{t} = \frac{K}{2}t$$

$$\tilde{\Delta} = \frac{4\Delta}{K} \tag{1.24}$$
$$\tilde{\omega}_0 = \frac{4\omega_0}{K}$$

we obtain the dimensionless system

$$\dot{q} = q\,(1 - \Delta - q + (1 - q)\cos\psi) \tag{1.25}$$
$$\dot{\psi} = \omega_0 - (1 + q)\sin\psi. \tag{1.26}$$

Here the overdot now means differentiation with respect to dimensionless time, and we have dropped all the tildes for convenience. For the rest of this section, all parameters will be assumed to be dimensionless (so there are implicitly tildes over them) unless stated otherwise.

1.4.2 Bifurcations of the incoherent state

The *incoherent state* is defined by $\rho_1 = \rho_2 = 0$, or by $q = 0$ in the phase plane formulation. The linearization of the incoherent state, however, is most easily performed in Cartesian coordinates using the formulation in Eqs. (1.16) and (1.17). We find the degenerate eigenvalues

$$\lambda_1 = \lambda_2 = 1 - \Delta - \sqrt{1 - \omega_0^2} \tag{1.27}$$
$$\lambda_3 = \lambda_4 = 1 - \Delta + \sqrt{1 - \omega_0^2}. \tag{1.28}$$

This degeneracy is expected because the origin is *always* a fixed point and because of the rotational invariance of that state. It follows that the incoherent state is stable if and only if the real parts of the eigenvalues are less than or equal to zero.

The boundary of stable incoherence therefore occurs when the following

conditions are met:

$$\begin{cases} \Delta = 1 + \sqrt{1 - \omega_0^2} & \text{for } \omega_0 \leq 1 \\ \Delta = 1 & \text{for } \omega_0 > 1. \end{cases} \tag{1.29}$$

These equations define the semicircle and the half-line shown in Fig. 1.2, labeled TC (for transcritical) and HB (for Hopf bifurcation), respectively. (Independent confirmation of these results can be obtained from the continuous formulation of Eq. (1.1) directly, as shown in the Appendix.) More precisely, we find that crossing the semicircle corresponds to a degenerate transcritical bifurcation, while crossing the half-line corresponds to a degenerate supercritical Hopf bifurcation.

In the latter case, the associated limit-cycle oscillation indicates that the angle ψ increases without bound; this reflects an increasing *difference* between the phases of the two 'sub'-order parameters of Eqs. (1.16, 1.17). In terms of the original model, this means that the oscillator population splits into two counter-rotating groups, each consisting of a macroscopic number of oscillators with natural frequencies close to one of the two peaks of $g(\omega)$. Within each group the oscillators are frequency-locked. Outside the groups the oscillators remain desynchronized, drifting relative to one another and to the locked groups. This is the state Crawford [10] called a *standing wave*. Intuitively speaking, it occurs when the two humps in the frequency distribution are sufficiently far apart relative to their widths. In Kuramoto's vivid terminology [19], the population has spontaneously condensed into "a coupled pair of giant oscillators."

1.4.3 Fixed point solutions and saddle-node bifurcations

Along with the trivial incoherent state $q = 0$, the other fixed points of Eqs. (1.25, 1.26) satisfy $1 - \Delta - q = (q - 1)\cos\psi$, and $\omega_0 = (q + 1)\sin\psi$. Using trigonometric identities, we obtain

$$1 = \left(\frac{\omega_0}{q+1}\right)^2 + \left(\frac{1-\Delta-q}{q-1}\right)^2, \tag{1.30}$$

or equivalently,

$$\omega_0 = \pm\frac{1+q}{1-q}\sqrt{\Delta(2-2q-\Delta)}. \tag{1.31}$$

Thus, the fixed point surface $q = q(\omega_0, \Delta)$ is defined implicitly. It can be single- or double-valued as a function of ω_0 for fixed Δ. To see this, consider how ω_0 behaves as $q \to 0^+$. We find that

$$\omega_0 \sim \sqrt{\Delta(2-\Delta)}\left[1 + \frac{3-2\Delta}{2-\Delta}q + O(q^2)\right], \tag{1.32}$$

from which we observe that the behavior changes qualitatively at $\Delta = 3/2$, as shown in Fig. 1.3.

The surface defined by $\rho = \rho(\omega_0, \Delta)$ can be plotted parametrically using ρ and Δ, as is seen in Fig. 1.4. The fold in the surface corresponds to a saddle-node bifurcation. Plots of the phase portrait of (q, ψ) reveal that the upper branch of the double-valued surface in Fig. 1.3 corresponds to sinks, and the lower branch to saddle points; see Fig. 1.2 (c), (d), and (g).

In physical terms, the sink represents a stable *partially synchronized state*, which is familiar from the classic Kuramoto model with a unimodal distribution [19, 44, 37, 4]. The oscillators whose natural frequencies are closest to the center of the frequency distribution $g(\omega)$ become rigidly locked, and maintain constant

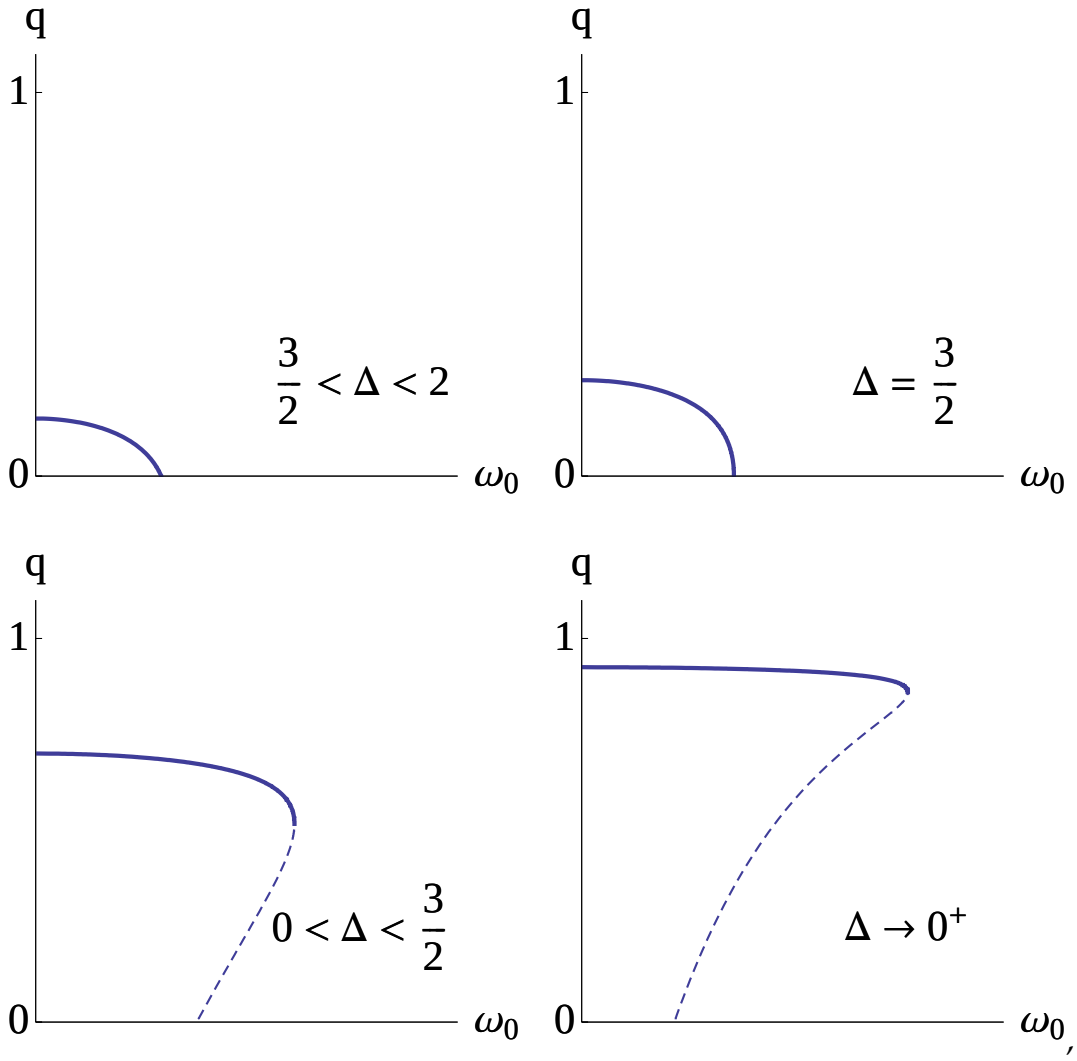

Figure 1.3: Saddle-node bifurcation: at $\Delta = 3/2$, q becomes double-valued.

phase relationships among themselves—in this sense, they act collectively like a "single giant oscillator," as Kuramoto [19] put it. Meanwhile the oscillators in the tails of the distribution drift relative to the locked group, which is why one describes the synchronization as being only partial.

The saddle points also represent partially synchronized states, though of course they are unstable. Nevertheless they play an important role in the dy-

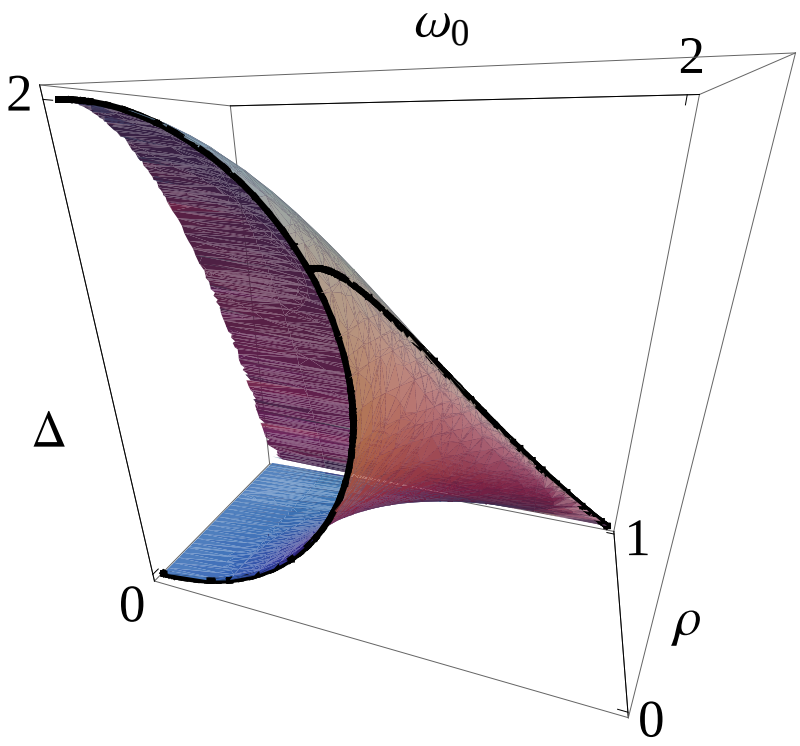

Figure 1.4: Fixed point surface. Bifurcation curves at the origin and the saddle-node curve are emphasized in black.

namics because they can annihilate the stable partially synchronized states; this happens in a saddle-node bifurcation along the fold mentioned above. To calculate its location analytically, we use (1.31) and impose the condition for a turning point, $\partial\omega_0/\partial q = 0$, which yields

$$q^2 - 4q + 3 - 2\Delta = 0. \tag{1.33}$$

Eliminating q from this equation using (1.31), we obtain the equation for the saddle-node bifurcation curve

$$\omega_0 = \sqrt{2 - 10\Delta - \Delta^2 + 2(1 + 2\Delta)^{3/2}}. \tag{1.34}$$

This curve is labeled SN in Fig. 1.2. Its intersection with the semicircle TC occurs

at $(\omega_0, \Delta) = (\frac{\sqrt{3}}{2}, \frac{3}{2})$, and is labeled B in the figure. Note also that point C in the figure is *not* a Takens-Bagdanov point, as the saddle-node and Hopf bifurcations occur at different locations in the state space; see Figs. 1.2 (a) and (g).

1.4.4 Bistability, homoclinic bifurcations, and SNIPER

An examination of the dynamics corresponding to the approximately triangular parameter space region ABC in Fig. 1.2 shows bistability. More specifically, we find that the stable incoherent fixed point coexists with the stable partially synchronized state produced by the saddle-node bifurcation described above, as shown in the state-space plot in Fig. 1.2(c).

Further study of these state-space plots led us to the homoclinic bifurcation curve marked HC, which was obtained numerically. The coexistence of states continues into region ACD, where we found that the stable partially synchronized state now coexists with the stable limit cycle created at the Hopf curve. (See Fig. 1.2(g).) This limit cycle is then destroyed by crossing the homoclinic curve, which is bounded by point A on one side and by point D on the other.

At point D, the homoclinic curve merges with the saddle-node curve. This codimension-two bifurcation, occurring at approximately (1.3589, 0.7483), is known as a saddle-node-loop [13, 46]. Below D, however, the saddle-node curve exhibits an interesting feature: the saddle-node bifurcation occurs on an invariant closed curve. This bifurcation scenario is known as a saddle-node infinite-period bifurcation, or in short, *SNIPER*. If we traverse the SNIPER curve from left to right, the sink and saddle (the stable and unstable partially synchronized states) coalesce, creating a loop with infinite period. Beyond that, a stable limit

cycle then appears—see Figs. 1.2 (d), (e), and (f).

In conclusion, we have identified six distinct regions in parameter space and have identified the bifurcations that occur at the boundaries.

1.5 Transverse Stability

Our analysis so far has been based on several simplifying assumptions. First, we restricted attention to a special family of oscillator distribution functions $f(\theta, \omega, t)$ and a bimodal Lorentzian form for $g(\omega)$, which enabled us to reduce the original infinite-dimensional system to a three-dimensional system of ODEs, Eqs. (1.18-1.20). Second, we considered only symmetric solutions of these ODEs, by assuming $\rho_1 = \rho_2$; this further decreased the dimensionality from three to two.

The next two sections test the validity of these assumptions. We begin here by showing that the non-zero fixed point attractor (the stable partially synchronized state) and the limit cycle attractor (the standing wave state) for Eqns. (1.25, 1.26) are transversely stable to small symmetry-breaking perturbations, i.e., perturbations off the invariant manifold defined by $\rho_1 = \rho_2$. This does not rule out the possible existence of attractors off this manifold, but it does mean that the attractors in the two-dimensional symmetric manifold are guaranteed to constitute attractors in the three-dimensional ODE system (1.18-1.20).

Let $\kappa = K/4$ and consider the reduced governing equations (1.18-1.20) without symmetry. Introducing the longitudinal and transversal variables

$$\rho_{\|} = \frac{1}{2}(\rho_1 + \rho_2)$$

$$\rho_\perp \;=\; \frac{1}{2}(\rho_1 - \rho_2), \tag{1.35}$$

and substituting these into (1.18-1.20), we derive the equation for the transversal component

$$\dot{\rho}_\perp \;=\; \rho_\perp\Big[(\kappa - \Delta) - \kappa(3\rho_\parallel^2 + \rho_\perp^2) - \kappa\cos\psi(1 + \rho_\parallel^2 - \rho_\perp^2)\Big],$$

which describes the order parameter dynamics off the symmetric manifold.

To simplify the notation, let $q_\parallel = \rho_\parallel^2$ and $q_\perp = \rho_\perp^2$ and scale the system using Eqs. (1.24), as before. Linearization and evaluation at the asymptotic solution denoted by (q_0, ψ_0), which may be either a fixed point or a limit cycle, yields the variational equation

$$\delta\dot{q}_\perp \;=\; \lambda_\perp \delta q_\perp \tag{1.36}$$

where

$$\lambda_\perp \;=\; 1 - \Delta - 3q_0 - (1 + q_0)\cos\psi_0. \tag{1.37}$$

Observe that $\delta q_\parallel$ and $\delta\psi$ do not appear in linear order on the right hand side of (1.36). This decoupling implies that $\lambda_\perp$ is the eigenvalue associated with the transverse perturbation $\delta q_\perp$, in the case where q_0 is a fixed point. Similarly, if q_0 is a limit cycle, the Floquet exponent associated with $\delta q_\perp$ is simply $\langle\lambda_\perp\rangle$, where the brackets denote a time average over one period. Hence the fixed point will be transversely stable if $\lambda_\perp < 0$. The analogous condition for the limit cycle is $\langle\lambda_\perp\rangle < 0$.

1.5.1 Fixed point stability

To test the transverse stability of sinks for the two-dimensional flow, we solve Eq. (1.25) for fixed points and obtain

$$0 \quad = \quad 1 - \Delta - q_0 + (1 - q_0)\cos\psi_0. \tag{1.38}$$

Subtracting this from (1.37), we find

$$\lambda_\perp \quad = \quad -2(q_0 + \cos\psi_0). \tag{1.39}$$

Hence $\cos\psi_0 > 0$ is a sufficient condition for transverse stability. But at a non-trivial fixed point,

$$\cos\psi_0 \quad = \quad \frac{1 - (\Delta + q_0)}{q_0 - 1}, \tag{1.40}$$

so the transverse stability condition is equivalent to $q_0 + \Delta > 1$.

We claim that this inequality holds everywhere on the upper branch of the fixed point surface (1.31). Obviously the inequality is satisfied at all points where $\Delta > 1$. For all other cases, consider the turning point from Fig. 1.3 defined by $q_{sn} = 2 \pm \sqrt{1 + 2\Delta}$. Since the function of interest, $Q(\Delta) \equiv q_{sn} + \Delta$, has a global minimum with $Q(0) = 1$, and q_{sn} is independent of ω_0 (at fixed Δ), it is a lower bound for all $q(\omega_0)$ on the upper sheet of the fixed point surface, provided that $q(\omega_0)$ is monotonically decreasing on the interval of $[0, \omega_{sn}]$. In fact, it is easier to establish that $0 > \partial\omega_0/\partial q = \Delta/D(q^2 - 4q + 3 - 2\Delta)$ with $D = (q-1)^2\sqrt{2\Delta - 2q\Delta - \Delta^2}$; the latter expression is positive, and $q^2 - 4q + 3 - 2\Delta < 0$ whenever $1 > q > q_{sn}$. Thus transverse stability for the nodes on the fixed point surface follows.

1.5.2 Limit cycle stability

To examine the transverse linear stability of the limit cycle, we calculate the transverse Floquet exponent by averaging the eigenvalue over the period of one oscillation:

$$\langle \lambda_\perp \rangle \quad = \quad 1 - \Delta - 3\langle q_0 \rangle - (\langle \cos\psi_0 \rangle + \langle q_0 \cos\psi_0 \rangle)\,. \tag{1.41}$$

In order to render this expression definite, we rewrite Eq. (1.25) in terms of the limit cycle solution (q_0, ψ_0):

$$\frac{d}{dt}(\ln q_0) \quad = \quad 1 - \Delta - q_0 + (1 - q_0)\cos\psi_0. \tag{1.42}$$

Periodicity on the limit cycle guarantees $\langle \frac{d}{dt} \ln q_0 \rangle = 0$, and so we have

$$0 \quad = \quad 1 - \Delta - \langle q_0 \rangle + \langle (1 - q_0)\cos\psi_0 \rangle, \tag{1.43}$$

which we subtract from the averaged eigenvalue to yield

$$\langle \lambda_\perp \rangle \quad = \quad -2(\langle q_0 \rangle + \langle \cos\psi_0 \rangle). \tag{1.44}$$

Although we are not able to analytically demonstrate that $\langle \lambda_\perp \rangle$ in (1.44) is negative, we have calculated $\langle q_0 \rangle$ and $\langle \cos\psi_0 \rangle$ numerically for the limit cycle attractors of Eqs. (1.18-1.20). This was done for 2500 parameter values corresponding to a grid in dimensionless parameter space, by sampling 50 evenly spaced values $\omega \in [0.01, 2.5]$ and $\Delta \in [0.01, 2.1]$. The simulations were run with $N = 1024$ oscillators. In all the cases that we tested, we found that $\langle \lambda_\perp \rangle < 0$.

1.6 Numerical Experiments

All of the results described above were obtained using the reduced ODE models derived in Sec. 1.3 B and C, and are therefore subject to the restrictions described

therein. It is therefore reasonable to ask if these results agree with the dynamics of the original system given in Eq. (1.1). To check this, a series of direct simulations of Eq. (1.1) using $N = 10,000$ oscillators and fourth-order Runge-Kutta numerical integration were performed.

First, we compared solutions of Eq. (1.1) with those of our reduced system Eqs. (1.22, 1.23) in the region where we predicted the coexistence of attractors. For example, we show in Fig. 1.5 a bifurcation diagram computed along the line $4\omega_0/K = 1.092$ that traverses the region ABCD in Fig. 1.2. (Note that here and for the rest of the paper, we revert to using the original, dimensional form of the variables.) The vertical lines in Fig. 1.5 indicate the locations of the bifurcations that were identified using the ODE models. For each point plotted, the simulation was run until the order parameter exhibited its time-asymptotic behavior; this was then averaged over the subsequent 5000 time steps. Error bars denote standard deviation. Note in particular the hysteresis, as well as the point with the large error bar, indicating the predicted limit cycle behavior.

Next, we examined the behavior of Eq. (1.1) at 121 parameter values corresponding to an 11×11 regular grid superimposed on Fig. 1.2, ranging from 0.1 to 2.1 at intervals of 0.2 on each axis. (In all cases, K was set to 1, and Δ and ω_0 were varied.) An additional series was run using a smaller grid (from 0.6 to 1.6 at intervals of 0.1 on each axis), to focus on the vicinity of region ABCD in Fig. 1.2. Initial conditions were chosen systematically in 13 different ways, as follows:

1. The oscillator phases were uniformly distributed around the circle, so that the overall order parameter had magnitude $r = 0$.
2. The oscillators were all placed in phase at the same randomly chosen angle

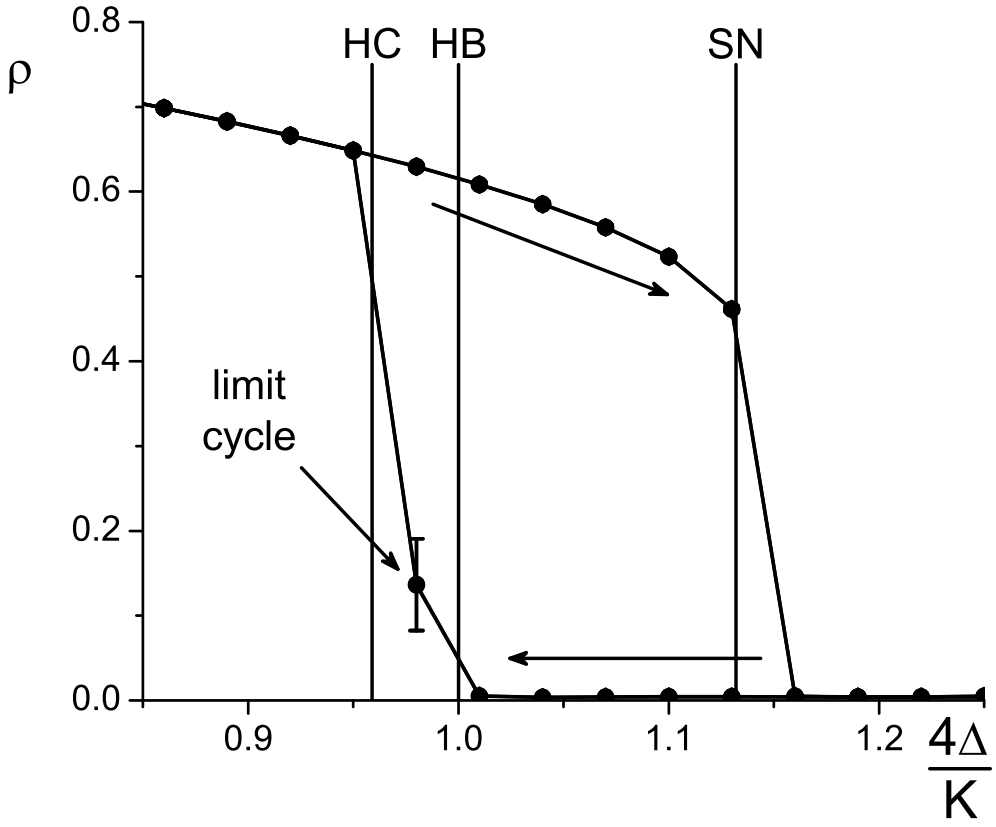

Figure 1.5: Hysteresis loop as observed when traversing the bistable regions shown in Fig. 1.2 in the directions shown (arrows) along the line at $4\omega_0/K = 1.092$. The data were obtained from a simulation of Equation (1.1) with $N = 10,000$ and $K = 1$. Vertical lines indicate where the reduced ODE models of Section 1.3 predict homoclinic (HC), degenerate Hopf (HB), and saddle-node (SN) bifurcations. Note that the point marked 'limit cycle' has a large error bar, reflecting the oscillations in the order parameter.

in $[0, 2\pi]$, so that $r = 1$.

3. The remaining 11 initial conditions were chosen by regarding the system as composed of two sub-populations, one for each Lorentzian in the bimodal distribution of frequencies, as in [5]. In one of the sub-populations,

the initial phases of the oscillators were chosen to be randomly spaced within the angular sector $[c + d, c - d]$, where c was chosen randomly in $[0, 2\pi]$ and d was chosen at random such that the sub-order parameter magnitude r_1 = 0.1, 0.2, 0.3, 0.4, 0.5, 0.6, 0.7, 0.8, or 0.9 (all approximately). The result was that r_1 had one of these magnitudes and its phase was random in $[0, 2\pi]$. The same procedure was followed for the other sub-population, subject to the constraint that $r_1 \neq r_2$. Our idea here was to deliberately break the symmetry of the system initially, to test whether it would be attracted back to the symmetric subspace defined by Eq. (1.21).

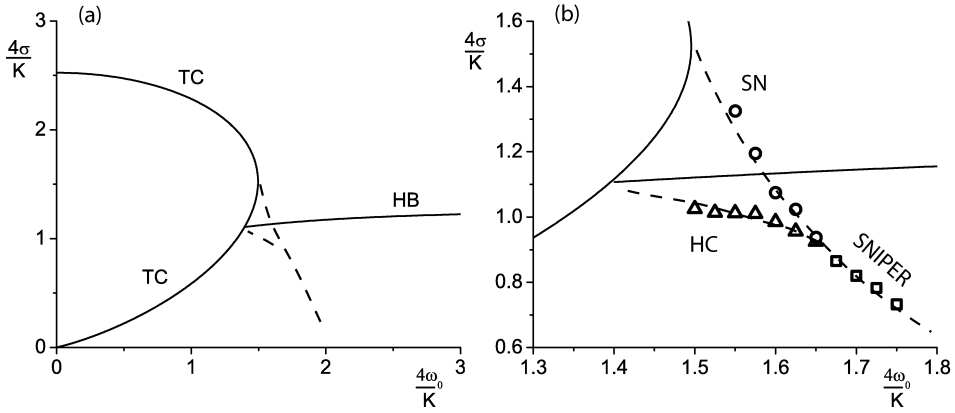

Figure 1.6: (a) Bifurcation diagram for the Kuramoto system with a bimodal frequency distribution consisting of two equally weighted Gaussians. All the features in Fig. 1.2 are present, but are somewhat distorted. The transcritical (TC) and (degenerate) Hopf curves (HB) were obtained as described in the Appendix. The dotted lines represent conjectured saddle-node, homoclinic, and SNIPER curves. These are based on the numerically-observed bifurcations shown in (b), which is a magnification of the central region of (a). The symbols represent saddle-node (circles), homoclinic (triangles), and SNIPER (squares) bifurcations.

In all the cases we examined, no discrepancies were found between the simulations and the predicted behavior. Although these tests were not exhaustive,

and certainly do not constitute a mathematical proof, they are consistent with the conjecture that no additional attractors beyond those described in Section III exist.

We then investigated the generality of our results by replacing the bimodal Lorentzian natural frequency distribution, Eq. (1.2), with the sum of two Gaussians:

$$g(\omega) = \frac{1}{\sigma\sqrt{2\pi}}\left(e^{-\frac{(\omega-\omega_0)^2}{2\sigma^2}} + e^{-\frac{(\omega+\omega_0)^2}{2\sigma^2}}\right) \tag{1.45}$$

and computing the corresponding bifurcation diagram analogous to Fig. 1.2. The results are shown in Fig. 1.6. The transcritical (TC) and degenerate Hopf bifurcation (HB) curves were obtained using the continuous formulation of Eq. (1.1); see the Appendix for details. In addition, saddle-node, homoclinic, and SNIPER bifurcations were numerically observed at several parameter values, and based on these data, we estimated the location of the corresponding curves (dashed lines). All the features of Fig. 1.2 are preserved, but the curves are somewhat distorted.

1.7 Discussion

We conclude by relating our work to three previous studies, and then offer suggestions for further research, both theoretical and experimental.

1.7.1 Kuramoto's conjectures

In his book on coupled oscillators, Kuramoto [19] speculated about how the transition from incoherence to mutual synchronization might be modified if the oscillators' natural frequencies were bimodally distributed across the population. On pp.75–76 of Ref. [19], he wrote "So far, the nucleation has been supposed to be initiated at the center of symmetry of g. This does not seem to be true, however, when g is concave there." His reasoning was that for a bimodal system, synchrony would be more likely to start at the peaks of g. If that were true, it would mean that a system with two equal peaks would go directly from incoherence to having two synchronized clusters of oscillators, or what we have called the standing wave state, as the coupling K is increased. The critical coupling at which this transition would occur, he argued, should be $K_c = 2/(\pi g(\omega_{\max}))$, analogous to his earlier result for the unimodal case. According to this scenario, the synchronized clusters would be tiny at onset, comprised only of oscillators with natural frequencies near the peaks of $g(\omega)$. Because of their small size, Kuramoto claimed these clusters "will behave almost independently of each other." With further increases in K, however, the clusters "will come to behave like a coupled pair of giant oscillators, and for even stronger coupling they will eventually be entrained to each other to form a single giant oscillator." (This is what we have called the partially synchronized state.)

Let us now re-examine Kuramoto's conjectures in light of our analytical and numerical results, as summarized in Fig. 1.7(a). For a fair comparison, we must assume that g is concave at its center frequency $\omega = 0$; for the bimodal Lorentzian (Eq. (1.2), this is equivalent to $\omega_0/\Delta > 1/\sqrt{3}$. (Otherwise g is unimodal and incoherence bifurcates to partial synchronization as K is in-

creased, consistent with Kuramoto's classic result as well as the lowest portion of Fig. 1.7(a).)

So restricting attention from now on to the upper part of Fig.1.7(a) where $\omega_0/\Delta > 1/\sqrt{3}$, what actually happens as K increases? Was Kuramoto right that the bifurcation sequence is always incoherence → standing wave → partial synchronization?

No. For ω_0/Δ between $1/\sqrt{3}$ and 1 (meaning the distribution is just barely bimodal), incoherence bifurcates directly to partial synchronization—the "single giant oscillator" state—without ever passing through an intermediate standing wave state. In effect, the system still behaves as if it were unimodal. But there is one new wrinkle: we now see hysteresis in the transition between incoherence and partial synchronization, as reflected by the lower bistable region in Fig. 1.7(a).

Is there any part of Fig. 1.7(a) where Kuramoto's scenario really does occur? Yes—but it requires that the peaks of g be sufficiently well separated. Specifically, suppose $\omega_0/\Delta > 1.81\ldots$, the value at the codimension-2 saddle-node-loop point where the homoclinic and SNIPER curves meet (i.e., point D in Fig. 1.2). In this regime everything behaves as Kuramoto predicted.

An additional subtlety occurs in the intermediate regime where the peaks of g are neither too far apart nor too close together. Suppose that $1 < \omega_0/\Delta < 1.81\ldots$. Here the system shows a different form of hysteresis. The bifurcations occur in the sequence that Kuramoto guessed as K increases, but *not* on the return path. Instead, the system skips the standing wave state and dissolves directly from partial synchronization to incoherence as K is decreased.

Finally we note that Kuramoto's conjectured formula $K_c = 2/(\pi g(\omega_{\max}))$ is incorrect, although it becomes asymptotically valid in the limit of widely separated peaks. Specifically, his prediction is equivalent to $K_c = \frac{8\Delta}{1+\sqrt{1+(\Delta/\omega_0)^2}} \sim 4\Delta(1 - \frac{1}{4}(\Delta/\omega_0)^2)$, which approaches the correct result $K_c = 4\Delta$ as $\omega_0/\Delta \to \infty$.

1.7.2 Crawford's center manifold analysis

Crawford [10] obtained the first mathematical results for the system studied in this paper. Using center manifold theory, he calculated the weakly nonlinear behavior of the infinite-dimensional system in the neighborhood of the incoherent state. From this he derived the stability boundary of incoherence. His analysis also included the effects of white noise in the governing equations.

Figure 1.7(b), reproduced from Fig. 4 in Ref. [10], summarizes Crawford's findings. Here D is the noise strength (note: our analysis is limited to $D = 0$), ϵ is the width of the Lorentzians (equivalent to Δ in our notation), and $\pm\omega_0$ are the center frequencies of the Lorentzians (as here). The dashed line in Fig. 1.7(b) shows Crawford's schematic depiction of the unknown stability boundary between the standing waves and the partially synchronized state. He suggested a strategy for calculating this boundary, and highlighted it as an open problem, writing in the figure caption, "...the precise nature and location of this boundary have not been determined." Our results, summarized in Figs. 1.2 and Fig. 1.7(a), now fill in the parts that were missing from Crawford's analysis.

1.7.3 Stochastic model of Bonilla et al.

In a series of papers (see [4] for a review), Bonilla and his colleagues have explored what happens if one replaces the Lorentzians in the frequency distribution with δ-functions, and adds white noise to the governing equations. The resulting system can be viewed as a stochastic counterpart of the model studied here; in effect, the noise blurs the δ-functions into bell-shaped distributions analogous to Lorentzians or Guassians. And indeed, the system shows much of the same phenomenology as seen here: incoherence, partially synchronized

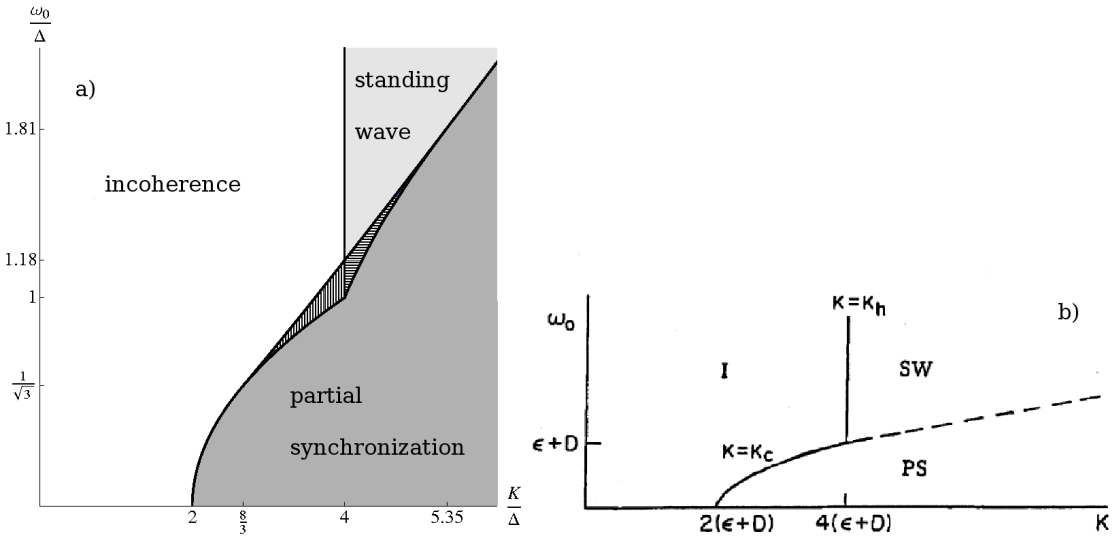

Figure 1.7: Stability diagram. (a) Results from our analysis, showing the long-term behavior in each region of parameter space. *White*: incoherence; *dark gray*: partial synchronization; *light gray*: standing wave (limit cycles); *vertical lines*: coexistence of incoherent and partially synchronized states; *horizontal lines*: coexistence of partial synchronization and standing waves. (b): Crawford's bifurcation diagram in [10]. In our study there is no noise, and so the diffusion is $D = 0$. Crawford's ϵ corresponds to our Δ. *I*: Incoherent states, *PS*: partially synchronized, *SW*: standing wave, equivalent to what we describe as two counter-rotating groups of oscillators. (Reprinted from [10] with permission of Springer Verlag.)

states, standing waves, and bistability [4].

However, a complete bifurcation diagram analogous to Fig. 1.2 has not yet been worked out for this model. The difficulty is that no counterpart of the ansatz (1.11) has been found; the stochastic problem is governed by a second-order Fokker-Planck equation, not a first-order continuity equation, and the Ott-Antonsen ansatz (1.11) no longer works in this case. Perhaps there is some way to generalize the ansatz appropriately so as to reduce the stochastic model to a low-dimensional system, but for now this remains an open problem.

1.7.4 Directions for future research

There are several other questions suggested by the work described here.

Validity of reduction method

The most important open problem is to clarify the scope and limits of the Ott-Antonsen method used in Sec. 1.3.2. Under what conditions is it valid to assume that the infinite-dimensional Kuramoto model can be replaced by the low-dimensional dynamical system implied by the Ott-Antonsen ansatz? Or to ask it another way, when do all the attractors of the infinite-dimensional system lie in the low-dimensional invariant manifold corresponding to this ansatz?

This question has now become particularly pressing, because two counterexamples have recently come to light in which the Ott-Antonsen method [38] gives an incomplete account of the full system's dynamics. When the method was applied to the problem of chimera states for two interacting populations of

identical phase oscillators, it predicted only stationary and periodic chimeras [1], whereas subsequent numerical experiments revealed that quasiperiodic chimeras can also exist and be stable [41]. Likewise, chaotic states are known to emerge from a wide class of initial conditions for series arrays of identical overdamped Josephson junctions coupled through a resistive load [12, 47]. Yet the Ott-Antonsen ansatz cannot account for these chaotic states, because the reduced ODE system turns out to be only two dimensional [34, 31].

What makes this all the more puzzling is that the method works so well in other cases. It seems to give a full inventory of the attractors for the bimodal Kuramoto model studied here, as well as for the unimodal Kuramoto model in its original form [18, 19, 38] or with external periodic forcing [38, 40, 9].

So we are left in the unsatisfying position of not knowing when the method works, or why. In some cases it (apparently) captures all the attractors, while in other cases it does not. How does one make sense of all this?

A possible clue is that in all the cases where the method has so far been successful, the individual oscillators were chosen to have randomly distributed frequencies; whereas in the cases where it failed, the oscillators were *identical*. Perhaps the mixing induced by frequency dispersion is somehow relevant here?

A resolution of these issues may come from a new analytical approach. Pikovsky and Rosenblum [41] and Mirollo, Marvel and Strogatz [34] have independently shown how to place the Ott-Antonsen ansatz [38] in a more general mathematical framework by relating it to the group of Mobius transformations [34, 11] or, equivalently, to a trigonometric transformation [41] originally introduced in the study of Josephson arrays [47]. This approach includes the

Ott-Antonsen ansatz as a special case, but is more powerful in the sense that it provably captures *all* the dynamics of the full system, and it works for any N, not just in the infinite-N limit. The drawback is that the analysis becomes more complicated. It remains to be seen what conclusions can be drawn—and, perhaps, what longstanding problems can be solved—when this new approach is unleashed on the Kuramoto model and its many relatives.

Even in those instances where the Ott-Antonsen ansatz doesn't account for all the attractors of the full system, it can still provide useful information, for instance by giving at least some of the attractors and by easing the calculation of them. Moreover, the transient evolution from initial conditions off the Ott-Antonsen invariant manifold can yield interesting phenomena not captured by the ansatz, as discussed in Appendix C of [40].

Asymmetric bimodal distributions

Now returning to the specific problem of the bimodal Kuramoto model: What happens if the humps in the bimodal distribution have unequal weights? The analysis could proceed as in this paper, up to the point where we assumed symmetry between the two sub-populations. One would expect new phenomena such as traveling waves to arise because of the broken symmetry.

Finite-size effects

We have focused here exclusively on the infinite-N limit of the Kuramoto model. What happens when the number of oscillators is reduced? How do finite-size effects influence the bifurcation diagram? An analysis along the lines of [14, 8]

could be fruitful for investigating these questions.

Comparison with experiment

Finally, it would be interesting to test some of these theoretical ideas in real systems. One promising candidate is the electrochemical oscillator system studied by Kiss and colleagues [17], in which the frequency distribution can be bimodal or even multimodal [33].

1.8 Acknowledgments

This research was supported in part by NSF grant DMS-0412757 and ONR award N00014-07-0734.

APPENDIX

Alternative calculation of the boundary of stability for the incoherent state

The system in Eq. (1.1), together with the bimodal natural frequency distribution given in Eq. (1.2), can be expressed using the formulation in [5] as two interacting populations of oscillators. In this case, each population has a separate Lorenzian frequency distribution of width Δ and center frequency at ω_0 or $-\omega_0$, and the two-by-two matrix describing the relative coupling weights (i.e, Eq. (1) in [5]) has 1/2 in each entry. By postulating that a small perturbation to the incoherent state grows exponentially as e^{st}, and setting $s = i\nu$ for the marginally stable state, Eq. (9) of Ref. [5] gives the following expression for the critical coupling value K:

$$K = \frac{2(\Delta^2 - \nu^2 + \omega_0^2) + i(4\Delta\nu)}{\Delta + i\nu}. \tag{1.46}$$

The boundary of stability of the incoherent state is obtained by requiring that this expression be strictly real. One solution is obtained for $\nu = 0$, resulting in $K = 2(\Delta^2 + \omega_0^2)/\Delta$, which is equivalent to

$$\left(\frac{4\Delta}{K} - 1\right)^2 + \left(\frac{4\omega_0^2}{K}\right)^2 = 1. \tag{1.47}$$

This is the equation for the semicircle in Figure 1.2, corresponding to a transcritical bifurcation of the incoherent state. Another solution, obtained by assuming that $\nu \neq 0$ in Eq. (1.46) and requiring $\omega_0 \geq \Delta$, is $K = 4\Delta$. This is the equation for the half-line in Figure 1.2 corresponding to the degenerate Hopf bifurcation of the incoherent state.

If the bimodal natural frequency distribution is given by a sum of Gaussians of standard deviation σ and centers at $\pm\omega_0$, then the two-population approach outlined above leads to the following equation:

$$K = \sigma\sqrt{\frac{32}{\pi}}\left[F\left(\frac{\omega_0 - \nu}{\sqrt{2}\sigma}\right) - F\left(\frac{-\omega_0 - \nu}{\sqrt{2}\sigma}\right)\right]^{-1}, \tag{1.48}$$

where

$$F(z) = \frac{i}{\pi}\int_{-\infty}^{\infty}\frac{e^{-t^2}}{z - t}dt \tag{1.49}$$

is known as the Faddeeva function and can be computed numerically [48]. Once again requiring that K be real, two branches corresponding to ν being equal and not equal to zero can be obtained. These are the boundaries of stability of the incoherent state shown in Fig. 1.6.

CHAPTER 2

BISTABLE CHIMERAE ON A TRIANGULAR NETWORK OF OSCILLATOR POPULATIONS

2.1 Abstract

We study a triangular network of three populations of coupled phase oscillators with identical frequencies. The populations interact nonlocally, in the sense that all oscillators are coupled to one another, but more weakly to those in neighboring populations than to those in their own population. This triangular network is the simplest discretization of a continuous ring of oscillators. Yet it displays an unexpectedly different behavior: in contrast to the lone stable chimera observed in continuous rings of oscillators, we find that this system exhibits *two* coexisting stable chimerae. Both chimerae are, as usual, born through a saddle node bifurcation. As the coupling becomes increasingly local in nature they lose stability through a Hopf bifurcation, giving rise to breathing chimerae, which in turn get destroyed through a homoclinic bifurcation. Remarkably, one of the chimerae reemerges by a reversal of this scenario as we further increase the locality of the coupling, until it is annihilated through another saddle node bifurcation.

2.2 Introduction

While studying a continuum of identical oscillators on a ring with nonlocal coupling, Kuramoto *et al.* [20] discovered a remarkable state where the population of oscillators splits into two subpopulations, where one is synchronized and the other is desynchronized. This state was later dubbed a *chimera*, alluding to a monster in Greek mythology that consists of incongruous parts. Since then, several groups have explored the nonlinear dynamics of chimera states [20, 3, 2, 43, 15, 16, 1, 22, 36]. Their emergence on the ring was first analyzed by

Abrams and Strogatz [3, 2], who found that chimera states were born through a saddle node bifurcation, which appears to be the typical scenario for the emergence of chimerae on all network topologies investigated so far. Shima and Kuramoto [43] showed that chimerae also exist on 2D lattices with free boundaries, specifically in the shape of spiral waves: here, the center of the spiral, characterized by a topological defect, is replaced by a desynchronized core with finite positive radius.

Recently, a breakthrough in the analysis of these systems has been made possible by an ansatz discovered by Ott and Antonsen [38]. Abrams *et al.* [1] have investigated a system of two interacting populations of phase oscillators; this system is closely related to ours and we will discuss it later in more detail. Applying the Ott-Antonsen approach to the case of populations with identical oscillators, Abrams *et al.* [1] calculated the saddle node bifurcation for this system analytically and showed that the chimera states undergo a further change of stability and become *breathing chimerae* via a supercritical Hopf bifurcation. Their approach was further generalized and put into a formal mathematical context by two teams independently: Pikovsky and Rosenblum [41] related the Ott-Antonsen ansatz to a trigonometric transformation, originally introduced in the study of Josephson arrays [47]; and Marvel *et al.* [34] showed that the ansatz is related to the group of Möbius transformations. Both teams found that the dynamics of each population can be reduced exactly to a flow described by three variables plus constants of motion.

Other studies have been concerned with showing how chimera states would occur or behave in real world systems: Omel'chenko *et al.* [36] show that a network of globally coupled oscillators, subjected to delayed feedback stimula-

tion with spatially decaying profile, generically induces chimera states; thereby they argue that chimera states indeed are a generic feature of coupled oscillator systems. Sethia *et al.* [42] also discuss a delay coupled system on a ring and discover the clustered chimera states. Makovetskiy and Markovetskii [26, 25] mention they found states similar to chimerae in systems of three level cellular automata in combination with spiral waves that appear in some lasing systems. The extension of the system with two nonlocally coupled populations discussed in [1] to the case of nonidentical oscillators, i.e. with heterogeneous natural frequencies, is discussed by Laing [22]; in the limit of global coupling, this system is equivalent to Kuramoto's problem with a bimodal distribution, and is studied by Martens *et al.* [28]. Laing shows that chimerae may both be destabilized and stabilized as the strength of heterogeneity (the width of the frequency distribution) of the oscillators is varied. In neuroscience, spatially localized "bumps" of neural activity are found in networks of spiking neurons; such states have been proposed as mechanisms for visual orientation tuning and working memory, and have been related to chimerae by some authors [23, 24].

An important open question is: on which topologies are chimera states possible? In other terms, can we classify the network structures that allow for chimerae? Even on one-dimensional domains the situation is unclear. It has been shown that chimerae may exist on a ring [20] with a continuum of oscillators, but it is not known whether chimerae can also exist on a finite line segment or the infinite line. The fact that we see chimerae in connection with spiral wave solutions on 2D lattices of oscillators [43, 30] is a hint that there indeed might be chimerae on 1D domains with nonperiodic, chain-like topologies.

Hoping that a lower dimensional approach would shed light on the mech-

anisms of emerging chimerae, we sought to answer this particular question by discretizing a one-dimensional domain into populations of identical oscillators. As in Abrams *et al.* [1], we assume that oscillators within a given population are coupled more strongly to each other than they are to those in neighboring populations, thus defining a spatial structure on the network. The simplest network that exhibits both chain-like and ring-like topology consists of three populations (Figure 2.1 (a)). By tuning a new structural parameter, we can continuously deform a rotationally symmetric (ring-like or "triangular") network into a less symmetric, chain-like structure.

While examining the simple case of a purely triangular network (Figure 2.1 (b)) we were surprised to find the *coexistence of two stable chimera attractors*. These attractors have different numbers of desynchronized populations (two in one case, and one in the other). This finding was unexpected because the ring with a continuum of oscillators [2, 3], sharing the same topological symmetry (rotational invariance), has only a single stable chimera state, dominated by a large desynchronized region interrupted by a small synchronized one. In this paper, we report the bistability of chimera attractors on a triangular network, and show that the resulting bifurcation scenario is a variant of that found for two populations [1]. This paper is wholly devoted to the triangular topology; in a companion paper we will discuss the impact of changing topology to a network with chain-like character [29].

The organization of the article is as follows. We introduce the governing equations in Section II and summarize the derivation to obtain the reduced set of equations, as described in [1]. Next we derive the equations implied by special symmetries allowing for chimera states. These are analyzed in Section III with

all their possible bifurcation scenarios. Section IV discusses our results in the context of numerical simulations. Finally, our findings are discussed in Section V. Additional results on stability of some simple symmetric states for arbitrary networks are outlined in the Appendix.

2.3 Governing equations

The governing equations are given by

$$\frac{d}{dt}\theta_i^\sigma = \omega + \sum_{\sigma'=1}^{3} \frac{K_{\sigma\sigma'}}{N_{\sigma'}} \sum_{j=1}^{N_{\sigma'}} \sin(\theta_j^{\sigma'} - \theta_i^\sigma - \alpha), \tag{2.1}$$

where the phases of the oscillators are defined by θ, i denotes the individual oscillators belonging to the population with index $\sigma = 1, 2, 3$, each of which has N_σ oscillators, and parameter α changes the way the phases of the oscillators attract one another.

The coupling kernel $K_{\sigma\sigma'}$ describes the strength between populations σ and σ'. The coupling strength is assumed to decay with increasing separation between the populations on the network. Within a population, the oscillators interact with strength $K_{\sigma\sigma'} = 1$. Neighboring populations couple more weakly, with strength $1 - A$ as displayed in Fig. 2.1 (b). We then have

$$K_{\sigma\sigma'} = \begin{pmatrix} 1 & 1-A & 1-A \\ 1-A & 1 & 1-A \\ 1-A & 1-A & 1 \end{pmatrix}. \tag{2.2}$$

In the case of $A = 0$, we retrieve the case of a globally coupled network. Thus A quantifies how 'far' we are from global coupling. This network has the same rotational symmetry as a continuum of oscillators on a ring, studied by [20, 2, 3],

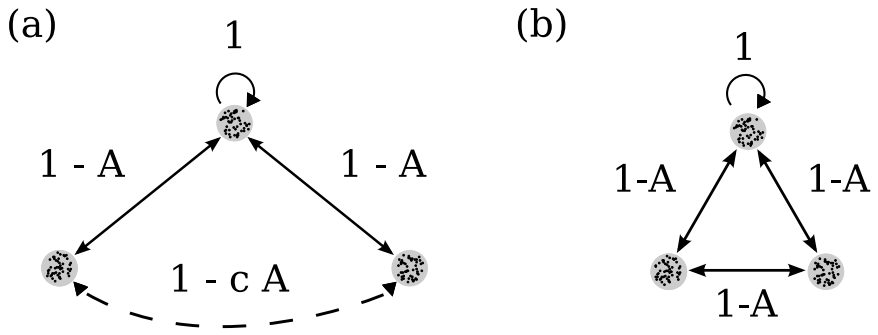

Figure 2.1: Networks of three populations of oscillators. The gray disks symbolize the populations of oscillators, populated by individual oscillators symbolized by black dots. Their bidirectional coupling is represented by black lines. (a) Chain-like general case with parameter c. (b) Triangular network structure, corresponding to $c = 1$. Each population has a self-coupling of unit strength 1, and is coupled to the neighboring populations with strength $1 - A$.

and generalizes the problem with two populations discussed by Abrams *et al.* [1].

2.3.1 Reduction to low-dimensional system

To make progress, we consider the limit of infinitely large populations, i.e. $N_\sigma \to \infty$. This allows us later to reduce the problem to a finite set of equations, using the ansatz introduced by Ott and Antonsen [38], outlined below. In this limit, it is natural to describe the dynamics of the system in terms of the oscillator density distribution $f^\sigma(\theta)$, which evolves according to the continuity equation

$$\frac{\partial f^\sigma}{\partial t} + \frac{\partial}{\partial \theta}(f^\sigma v^\sigma) \;=\; 0. \tag{2.3}$$

The velocity of the oscillators is then given by

$$v^{\sigma} = \omega + \sum_{\sigma'=1}^{3} K_{\sigma\sigma'} \int_0^{2\pi} \sin(\theta' - \theta - \alpha) f^{\sigma'}(\theta', t) d\theta'. \tag{2.4}$$

To keep the notation simple we denote θ_σ by θ and $\theta_{\sigma'}$ by θ'. It proves convenient to define a complex order parameter

$$z^{\sigma}(t) = \sum_{\sigma'=1}^{3} K_{\sigma\sigma'} \int_0^{2\pi} e^{i\theta'} f(\theta', t) d\theta', \tag{2.5}$$

which defines a weighted average over all oscillators; we therefore refer to this as the *global order parameter*. Following Kuramoto's footsteps [19, 21, 20], we rewrite the velocity in terms of the order parameter and find

$$\begin{aligned} v^{\sigma} &= \omega + \mathrm{Im}\left[e^{-i\theta} e^{-i\alpha} \sum_{\sigma'=1}^{3} K_{\sigma\sigma'} \int_0^{2\pi} e^{i\theta'} f(\theta', t) d\theta' \right] \\ &= \omega + \frac{1}{2i}\left[e^{-i\theta} e^{-i\alpha} z_{\sigma}(t) - e^{i\theta} e^{i\alpha} z_{\sigma}^{*}(t) \right]. \end{aligned} \tag{2.6}$$

Following Ott and Antonsen [38], we now restrict attention to a special class of density functions in the form of a Poisson kernel

$$f^{\sigma}(\theta, t) = \frac{1}{2\pi}\left\{ 1 + \left[\sum_{k=1}^{\infty} (a_{\sigma}(t) e^{i\theta})^k + c.c. \right] \right\}, \tag{2.7}$$

where c.c. is the complex conjugate of the expression under the sum. The implications of this special ansatz and its validity will be explained in more detail in Section 2.6. Substitution of f_σ and v_σ into the continuity equation (2.3) yields an exact solution, so long as a_σ evolves according to

$$0 = \dot{a}_{\sigma} + i\omega a_{\sigma} + \frac{1}{2} a_{\sigma}^2 z_{\sigma} e^{-i\alpha} - \frac{1}{2} z_{\sigma}^{*} e^{i\alpha}. \tag{2.8}$$

It remains to express the order parameter in terms of this ansatz. We find

$$z_{\sigma}(t) = \sum_{\sigma'=1}^{3} K_{\sigma\sigma'} a_{\sigma'}^{*}(t). \tag{2.9}$$

Finally, we express the amplitude a_σ in polar coordinates as

$$a_\sigma = \rho_\sigma e^{-i\phi_\sigma}.$$

By division of (2.8) by $e^{-i\phi_\sigma}$, we obtain

$$0 = \dot{\rho_\sigma} - i\dot{\phi_\sigma}\rho_\sigma + i\omega\rho_\sigma + \frac{1}{2}\rho_\sigma^2 \sum_{\sigma'=1}^{3} K_{\sigma\sigma'}\rho_{\sigma'} e^{i(\phi_{\sigma'}-\phi_\sigma-\alpha)} - \frac{1}{2}\sum_{\sigma'=1}^{3} K_{\sigma\sigma'}\rho_{\sigma'} e^{-i(\phi_{\sigma'}-\phi_\sigma-\alpha)},$$

and by separation of real and imaginary parts we eventually find

$$\begin{aligned}
\dot{\rho}_\sigma &= \frac{1-\rho_\sigma^2}{2}\sum_{\sigma'=1}^{3} K_{\sigma\sigma'}\rho_{\sigma'}\sin(\phi_{\sigma'}-\phi_\sigma+\beta), \\
\dot{\phi}_\sigma &= \omega - \frac{1+\rho_\sigma^2}{2\rho_\sigma}\sum_{\sigma'=1}^{3} K_{\sigma\sigma'}\rho_{\sigma'}\cos(\phi_{\sigma'}-\phi_\sigma+\beta),
\end{aligned} \tag{2.10}$$

where we introduce the definition

$$\beta = \pi/2 - \alpha. \tag{2.11}$$

These equations describe the dynamics of our system in terms of the variables a_σ. Notice that in contrast to z_σ, they do not represent averages over all populations, and therefore, we refer to them as *local order parameters*. Thus any synchronized population σ of oscillators is characterized by $\rho_\sigma = 1$. (These results are trivially generalized to the case of a network with arbitrarily many populations $\sigma = 1, 2, \ldots, N$.)

In what follows, we will make particular assumptions about the symmetries of the solutions that we expect to find. Then we will analyze existence, stability and bifurcations of the states of interest.

2.3.2 Manifold of Symmetric States (SDS and DSD)

To make progress on analyzing the chimera states, we will have to make certain symmetry assumptions. Recall that populations that are perfectly synchronized

have $\rho_\sigma = 1$. Desynchronized populations have $\rho_\sigma < 1$, and consist of oscillators that drift relative to one another and to the synchronized populations. Let S and D denote synchronized and desynchronized populations, respectively. Then in a triangular network, we can distinguish only two chimera states, namely SDS (sync-drift-sync) and DSD (drift-sync-drift); all other permutations of S and D give equivalent states because of the rotational invariance inherent to the triangular network.

Another class of solutions (of less interest to us) could be described as SSS. Here, all oscillators are in sync in a given population but the populations might have different synchronized phases ϕ_i. For a network involving only three populations, we may distinguish three such states, i.e. $\phi_1 = \phi_2 = \phi_3$, $\phi_1 = \phi_3 \neq \phi_2$ and the state where all phase angles are different. These solutions are analyzed in Appendix A. For now, we shall restrict ourselves to chimera states and their emergence in parameter space.

For the case of a triangle, the SDS state is defined via $\rho_1 = \rho_3 = 1$ and $\rho \equiv \rho_2 < 1$, whereas the DSD state has $\rho \equiv \rho_1 = \rho_3 < 1$ and $\rho_2 = 1$. The symmetry of our coupling kernel (2.2) in combination with $\rho_1 = \rho_3$ implies that $\phi_1 = \phi_3$ and hence populations 1 and 3 are phase-locked. We define the phase difference of the angular order parameter between the synchronized and desynchronized states by

$$\psi = \phi_1 - \phi_2 = \phi_3 - \phi_2. \tag{2.12}$$

Applying these symmetry assumptions to (2.10) and substituting the coupling kernel defined in (2.2), we obtain the equations describing the SDS states

$$\begin{aligned} \dot{\rho} &= \frac{1-\rho^2}{2}\left[2(1-A)\sin(\psi+\beta)+\rho\sin\beta\right], \\ \dot{\psi} &= -(2-A)\cos\beta-(1-A)\rho\cos(-\psi+\beta) \end{aligned}$$

$$+ \quad \frac{1+\rho^2}{2\rho}\left[2(1-A)\cos(\psi+\beta)+\rho\cos\beta\right], \tag{2.13}$$

and the DSD states

$$\begin{aligned}
\dot{\rho} &= \frac{1-\rho^2}{2}\left[(2-A)\rho\sin\beta+(1-A)\sin(-\psi+\beta)\right], \\
\dot{\psi} &= -\frac{1+\rho^2}{2\rho}\left[(2-A)\rho\cos\beta+(1-A)\cos(-\psi+\beta)\right] \\
&+ \quad 2(1-A)\rho\cos(\psi+\beta)+\cos\beta.
\end{aligned} \tag{2.14}$$

Note that these equations hold only if we restrict attention to symmetry-preserving perturbations. The fixed points of (2.13,2.14) correspond to phase-locked solutions of the original system (at the macroscopic level of the local order parameters).

By reduction of the full system of oscillators (2.1) to a low dimensional system for the local order parameters, we have cast our problem into a two dimensional system represented by Eqs. (2.13,2.14). This enables us to study the problem in the phase plane.

2.4 Analysis

2.4.1 Phase Portraits

Unfortunately, we cannot solve the equations for the SDS and DSD states in closed form. Before we get deeper into the matter of analyzing these states, let us get a quick intuition of their behavior by inspecting the phase planes of their corresponding equations, which will guide us in the subsequent analysis. Their phase portraits shown in Fig. 2.2 and Fig. 2.5 represent a sweep in parameter

space with increasing values of A while keeping the value of $\beta = 0.05$ constant (close to pure cosine coupling).

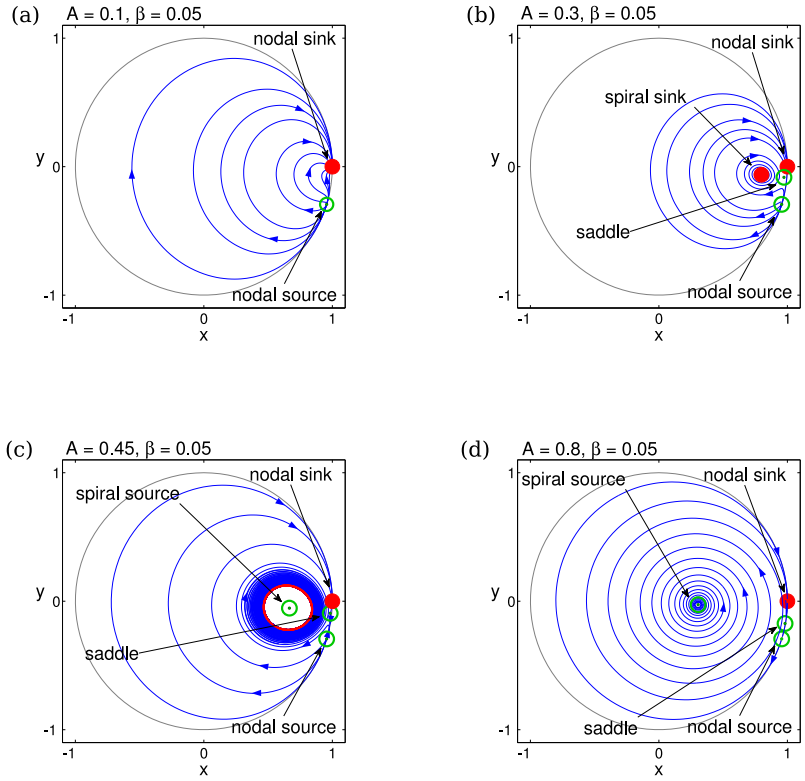

Figure 2.2: Phase portraits for the SDS chimera, with increasing values of A at constant β. The unit circle displayed in gray. Stable fixed points are shown as solid (red) and open (green) circles, respectively. Limit cycles are emphasized in red color. The point in $(\rho, \psi) = (1, 0)$ is a nodal sink. The position of the nodal source depends on β and moves in clockwise direction with growing values of β.

Let us first consider the SDS symmetry. For small values of A (close to global coupling), we only observe a nodal sink and source on the unit circle; these points correspond to the in-phase SSS solutions (Fig. 2.2(a)). Increasing A further, a saddle-node pair is born very close to the unit circle. For larger A,

the node moves closer to the origin, implying that the order of the desynchronized population decreases and the chimera state becomes more pronounced (if we instead increase the values of β, this critical point starts to move clockwise while getting closer to the origin). The node has become a stable spiral (Fig. 2.2(b)), and at a critical value of A, it loses stability through a Hopf bifurcation and a limit cycle is born (Fig. 2.2(c)). The amplitude of the order parameter ρ of the drifting population starts to oscillate, and is therefore called a *breathing chimera*. As we raise the value of A more, the limit cycle gains in amplitude until it collides with the saddle: the limit cycle is destroyed in a homoclinic bifurcation (Fig. 2.2(d)). The resulting bifurcation diagram is shown in Fig. 2.3. The saddle-node, Hopf and homoclinic bifurcation curves all intersect in a Takens-Bogdanov point with codimension two.

For the DSD symmetry, we observe a scenario that is qualitatively similar to the previous case. However, surprisingly, the whole scenario appears a second time in the upper part of the parameter plane, but now in reversed order, as shown in Fig. 2.4. We again sweep parameter space with increasing values of A while keeping β constant, as shown in Fig. 2.5. For all parameter values, we find two synchronized SSS solutions on the unit circle: one is a nodal sink in $(\rho, \psi) = (1, 0)$, but what in the SDS case before was a nodal source, is now a saddle. Also notice that a new fixed point has appeared in the left half of the unit circle in the form of a spiral source (Fig. 2.5(a)). This is the second, currently unstable, DSD chimera seen in the upper half of the bifurcation diagram. As A increases and the coupling becomes more local, a saddle-node pair is born in the right half of the unit circle (Fig. 2.5(b)); again, its node then becomes a spiral and loses stability as the coupling strength becomes more local, and the resulting limit cycle (Fig. 2.5(c-d)) gets ultimately destroyed in a homoclinic bifurcation

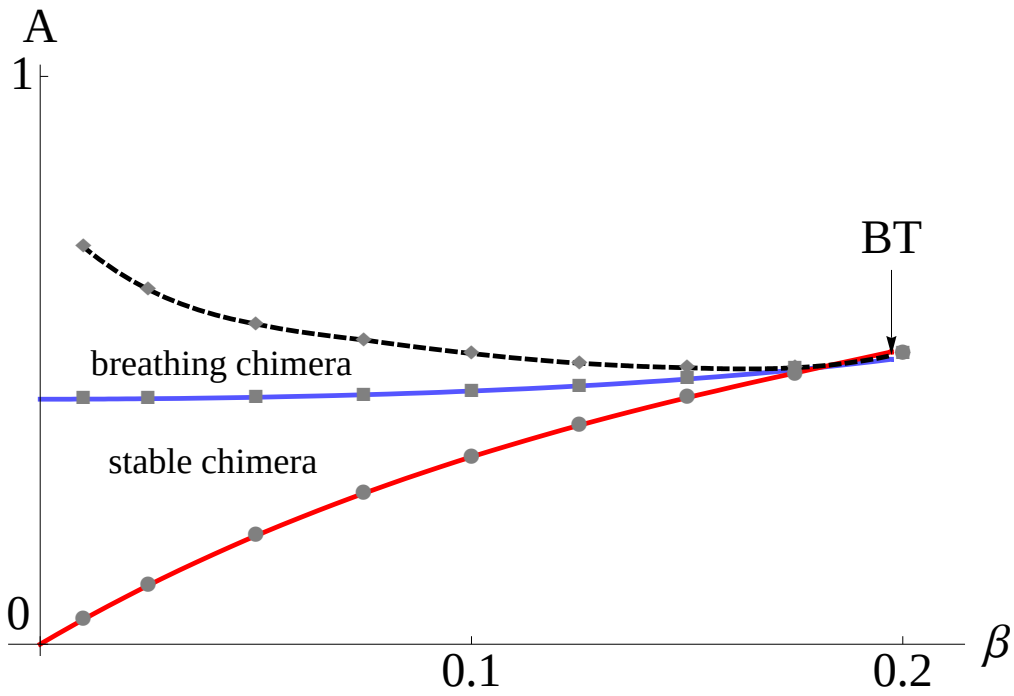

Figure 2.3: Bifurcation diagram for the *SDS* chimera. The curves we display are: the saddle-node curve (blue), the Hopf curve (red), and the homoclinic curve (black and dashed). Dots mark the bifurcation points obtained by inspection of the phase plane. The homoclinc curve (dashed black) is an interpolation based on these points, whereas all the solid curves were obtained analytically.

(Fig. 2.5(e)). Whereas one chimera has been rendered unstable, we observe that, above a critical A, a stable limit cycle has formed around the spiral source on the left half of the circle: the twin of the *DSD* chimera in its breathing mode has emerged (Fig. 2.5(e)). From here, the bifurcations happen in reversed order, the source becomes first a spiral node (Fig. 2.5(f)), i.e. a stable chimera, which is eventually annihilated in a saddle-node bifurcation. The resulting bifurcation diagram is seen in Fig. 2.4.

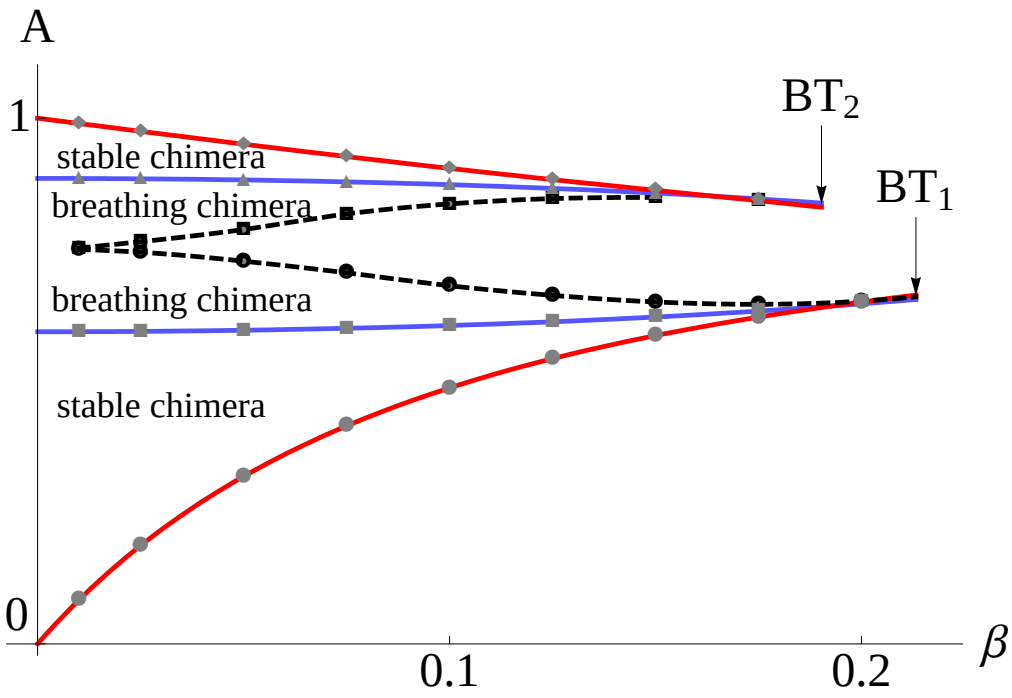

Figure 2.4: Bifurcation diagram for the *DSD* chimerae. The curves we display are: saddle-node curve (blue), Hopf curve (red), homoclinic curve (black and dashed). Dots mark the bifurcation points obtained by inspection of the phase plane. The homoclinc dashed curve is an interpolation based on these points, whereas all the solid curves are obtained analytically.

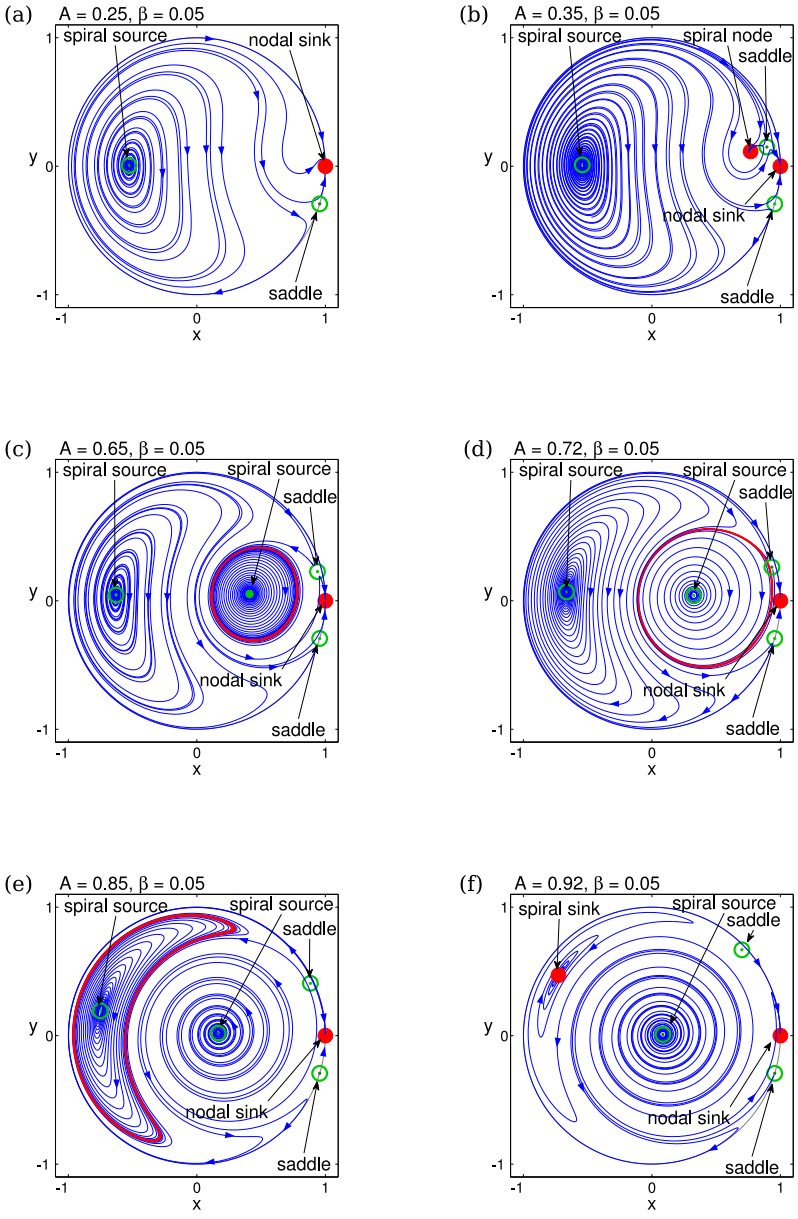

Figure 2.5: Phase portraits for the *DS D* chimerae, with increasing values of A at constant β. The unit circle is displayed in gray. Stable and unstable fixed points are shown as solid (red) and open (green) circles, respectively. Limit cycles are emphasized in red color. The point in $(\rho, \psi) = (1, 0)$ is a nodal sink. The position of the saddle depends on β and moves in clockwise direction with growing values of β.

2.4.2 Calculating the Bifurcation Curves

In order to calculate the saddle-node and Hopf curves of the SDS solutions, we must linearize (2.13) around the appropriate fixed point. This task amounts to solving the fixed point equations implied by Eqs. (2.13) and (2.14) simultaneously with the saddle node condition,

$$\det(J) = 0,$$

or with the Hopf condition,

$$\mathrm{tr}(J) = 0 \quad \text{and} \quad \det(J) > 0,$$

where J denotes the Jacobian of (2.13) or (2.14), respectively. For the SDS symmetry, we have

$$\begin{aligned}
J_{11} &= \frac{1}{2}\left[(1-3\rho^2)\sin\beta - 4(1-A)\rho\sin(\beta+\psi)\right], \\
J_{12} &= (1-A)(1-\rho^2)\cos(\beta+\psi), \\
J_{21} &= \frac{1}{\rho^2}\left[\cos\beta(\rho^3-(1-A)\cos\psi) - \sin\beta\sin\psi(2\rho^2-1)(1-A)\right], \\
J_{22} &= \frac{A-1}{\rho}\left[(1+2\rho^2)\cos\psi\sin\beta + \cos\beta\sin\psi\right].
\end{aligned}$$

The fixed point condition implied by (2.13) yields the nontrivial solution

$$\rho = 2(A-1)\csc\beta\sin(\beta+\psi). \tag{2.15}$$

Substitution of this expression into the fixed point condition for ψ results in

$$\begin{aligned}
0 &= (A-2)\cos\beta + \frac{1}{2}\csc(\beta+\psi)\sin\psi \\
&+ (1-A)^2\csc\beta\left[\sin 2\beta + 2(\cot\beta\sin^2\psi + \sin 2\psi)\right].
\end{aligned} \tag{2.16}$$

Unfortunately, this equation cannot be solved in closed form for ψ, which in turn would allow us to express A in terms of β. We settle therefore for a series

approach in A and ψ, as follows:

$$\psi = \sum_{k=0}^{N} p_k \beta^k + O(\beta^{N+1}) \tag{2.17}$$

$$A = \sum_{k=0}^{N} a_k \beta^k + O(\beta^{N+1}). \tag{2.18}$$

We substitute these two expressions into fixed point equation (2.16) and the saddle node condition, and solve the resulting equations for each power of β. This leads to the following expression for the saddle node curve:

$$\begin{aligned} A_{SN}(\beta) &= \frac{9}{2}\beta - \frac{63}{4}\beta^2 + \frac{195}{4}\beta^3 - \frac{2355}{16}\beta^4 + \frac{35283}{80}\beta^5 - \frac{210247}{160}\beta^6 \\ &+ \frac{872617}{224}\beta^7 - \frac{2949379}{256}\beta^8 + \frac{2744116261}{80640}\beta^9 + O(\beta^{10}). \end{aligned} \tag{2.19}$$

Using the Hopf condition and proceeding in the same way we also find the Hopf curve, approximated by

$$A_H(\beta) = 0.447153 + 1.34639\,\beta^2 + 8.34371\,\beta^4 + O(\beta^6).$$

The Takens-Bogdanov point is determined by numerically solving the saddle-node, Hopf and fixed point conditions simultaneously. It is located at

$$(\beta, A)_{SDS} = (0.1974, 0.5092) \tag{2.20}$$

The bifurcation curves for the DSD chimerae are obtained in an analogous procedure. Solving the equations expanded in series is now a bit trickier due to the coexistence of two branches. For brevity, we shall only summarize our findings. The two saddle node curves are approximated by

$$\begin{aligned} A_{SN,1}(\beta) &= 9\beta - 72\beta^2 + \frac{1059}{2}\beta^3 - 3855\beta^4 + \frac{1130943}{40}\beta^5 - \frac{1039276}{5}\beta^6 \\ &+ \frac{854234093}{560}\beta^7 - \frac{78311783}{7}\beta^8 + \frac{3309788681161}{40320}\beta^9 + O(\beta^{10}), \end{aligned} \tag{2.21}$$

$$A_{SN,2}(\beta) = 1 - \beta + \frac{31}{6}\beta^3 - \beta^4 - \frac{6421}{120}\beta^5 + O(\beta^6). \tag{2.22}$$

Unfortunately, the series approach for the lower second branch converges extremely slowly and doesn't match all the way to the Takens-Bogdanov point (even going to this high order doesn't help!). The hard work to find the series coefficients was however not all in vain: we find that a Padé approximant based on the above power series does already at order three an excellent job in matching the data points retrieved from the examination of the phase portraits. We have

$$A_{SN,2}(\beta) \approx \frac{9\beta + \frac{1521018}{301403}\beta^2 + \frac{287446827}{6028060}\beta^3}{1 + \frac{2580226}{301403}\beta + \frac{90123833}{6028060}\beta^2 + \frac{200207828}{4521045}\beta^3}. \quad (2.23)$$

Finally, the Hopf curves are approximated by

$$A_{H,1}(\beta) = 0.593737 + 1.14491\beta^2 + 4.55308\beta^4 + O(\beta^6), \quad (2.24)$$

$$A_{H,2}(\beta) = 0.885408 - 1.15074\beta^2 - 3.96289\beta^4 + O(\beta^6). \quad (2.25)$$

The Takens-Bogdanov points are located at

$$(\beta, A)_{DSD,1} = (0.2132, 0.6615) \quad (2.26)$$

$$(\beta, A)_{DSD,2} = (0.1903, 0.8359). \quad (2.27)$$

For all symmetries, we found an excellent agreement of our perturbative results with the bifurcation points obtained from inspection of the phase portraits. We did not derive an analytical expression for the homoclinic bifurcation curves; the curves shown in the Figs. 2.3 and 2.4 are based on data points obtained from inspecting the phase portraits while varying the parameters.

2.5 Numerical Simulations

We have obtained analytical results describing the dynamics of our triangular network of oscillator populations, using two different reductions: firstly, we re-

duced the governing Eqs. (2.1) using the Ott Antonsen method. And secondly, we have assumed that the system attains certain symmetry states that allow for chimera states; these symmetries need not be transversely stable to perturbations off the symmetry manifold. Thus, the equations obtained from these reductions may not necessarily account for the complete dynamics of the governing equations, and we checked if our analytical results agree with numerical simulations of the governing equations. We did this with a finite, but what may be considered a sufficiently large oscillator population.

We used two different methods to generate initial conditions that would lead to the appearance of chimera states. For either methods, the phases for the synchronized populations are given by $\phi_i^{\sigma,s} = 0$, w.l.o.g. Firstly, for the phases of the desynchronized populations we used an initial condition in the shape of a bump, specifically, a Gaussian distribution in the shape of $\phi_i^{\sigma,d} \sim \exp\left(-\gamma(i/N_\sigma - 1/2)^2\right)$, where we chose an appropriate decay rate γ. The second method was designed with the intention to place the system right on the Ott-Antonsen (OA) manifold. This was accomplished by generating a phase distribution that is consistent with the Poisson kernel (2.7). To achieve this, we solved the SDS and DSD Eqs. (2.13) and (2.14), respectively, for fixed points (ρ, ψ). This in turn, enables us to compute the Poisson distribution $f^\sigma(\theta, t)$ defined by (2.7), by using the definition of the order parameter, $a_\sigma = \rho_\sigma e^{-i\phi_\sigma}$. Because this function defines the probability with which oscillators populate a certain phase, we may use its inverse cumulative distribution function to construct from it a set of phases that is consistent with the OA-manifold. The system should remain close to the OA-manifold, because of its invariance. Unless mentioned otherwise, we used this latter method.

We first confirmed that the unreduced system would exhibit all types of chimerae predicted by our analysis, and that they would correspond to stable states, for various points in parameter space. These states were observed with both $N_\sigma = 20$ and $N_\sigma = 200$ oscillators per population. The observed behavior is that the system first goes through a tiny transient and reach an attracting state which was confirmed to be stable even for long computation times. The transient may be explained by the fact that the system due to its finite size can only be approximately on to the OA-manifold (or a member of the OA-family, as explained in the Discussion).

Next we checked if the critical parameter values of saddle node, Hopf and homoclinic bifurcation in the full system would be in accord with the critical values obtained from our theory, see Figs. 2.6 (a) and (b). In order to do so, we held the value of β fixed and continued a solution through 20 increasing values of A. To initiate the continuation we used an initial condition consistent with the OA-manifold.

In Fig. 2.6, we show fixed points and oscillation amplitudes of the order parameter, obtained analytically from (2.13) and (2.14), as dashed curves. Our simulation results are superposed, and were obtained as follows: First of all, to remove transient effects from our analysis, we only considered the last 2/5 of the computed time series. Instead of only detecting the global maximum and minimum of the series, we detected local maxima, shown as light gray dots, and minima, shown as dark gray dots. We chose to do this, because it would allows us to see the traces of new appearing periods, that potentially may occur in the unreduced, highly dimensional system. However, finite size fluctuations also cause small oscillations; this is the reason we see some small amount of

blurring in the data (For similar reasons, maxima and minima on the stable branch do not coincide.)

Despite these undesired effects, we can clearly demonstrate the onset of the Hopf and the homoclinic bifurcations in the simulation. Consider first the SDS chimera, shown in Fig. 2.6 (a). We expect that finite size effects affect the locations of all the bifurcation points. While we would have to compute at a higher resolution for the continuation to actually see this happen for the Hopf bifurcation, it is more apparent for the homoclinic bifurcation: the limit cycle oscillation brings the system periodically close to the saddle point (as is seen in the phase plane); therefore, the larger finite size fluctuations are, the more likely the system is to be kicked off the limit cycle and is instead attracted to the nearby all-in-phase SSS state on the unit circle. This is seen in Fig. 2.6 (a), where the limit cycle oscillation disappears at a smaller value of A than it does for the analytic result (sold curve indicates SSS state). The same behavior is observed for the DSD chimera in Fig. 2.6 (b), but much more pronounced: the system snaps to the in-phase state (solid curve) much earlier than expected for a continuous system of oscillators. Similarly, we can continue the solutions in reverse direction, and check that the chimera states are annihilated via a saddle node bifurcation; we don't show this in the Figure, but it indeed happens near the predicted value.

Whereas we easily managed to show DSD states in the lower half of the parameter plane, our attempts to place the system on the second DSD attractor had little success: for all trials the system would eventually reach the in-phase state. Increasing the number of populations didn't seem to remedy the matter, as one might be led to think from our previous experience; rather, the system

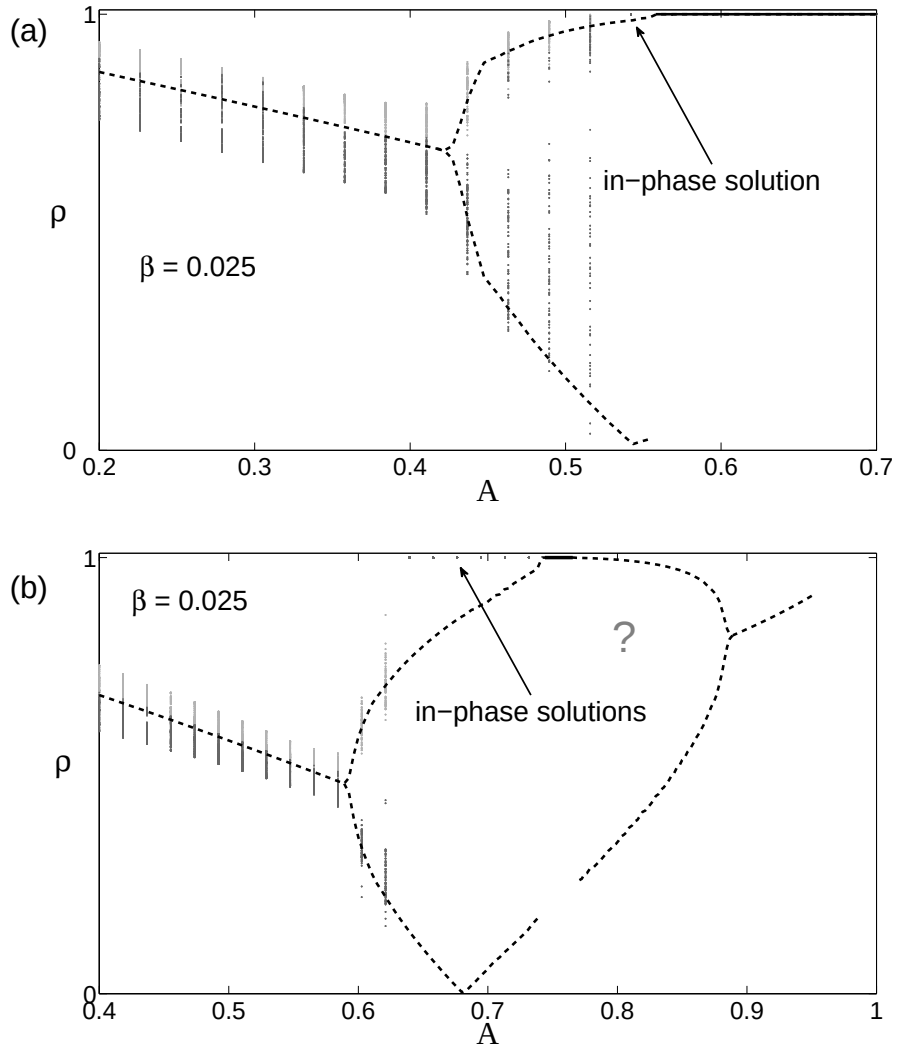

Figure 2.6: Bifurcation diagram obtained from numerical simulation, for the states SDS shown in (a) and DSD in (b). Light dots and dark circles correspond to the local maxima and minima, respectively, that are detected by the algorithm. The dashed curve represents the analytical result for the continuum case ($N \to \infty$). The computations were performed with $N_\sigma = 40$ oscillators per population for a simulation time of $T = 100$. (The kink in the lower left branch is an artefact from the limit cycle reaching into the lefthand side quadrants, as ρ is not measured relative to the limit cycle center but to the origin.)

would stay obediently in the DSD state for a little while and then suddenly jump into the in-phase state. However, it doesn't seem to be entirely clear whether the second attractor of the DSD state is inherently unstable, or if it is just very hard to stay on that manifold due to a combination of factors, given by finite size effects and the location, small size and special shape of the attractor (see the phase plane, Fig. 2.5). Specifically, in the case of a breathing state, the limit cycle is always very close to the invariant field defined by the in-phase state on the unit circle. In conclusion, it is likely that this second DSD attractor is unstable to either symmetry breaking perturbations or to perturbations off the OA-manifold.

2.6 Discussion

In conclusion, we have investigated a triangular network of populations with identical, sinusoidally coupled oscillators that are nonlocally coupled. As an approximation of the practical case of large populations, our analysis addresses the limiting case of populations with infinitely many oscillators per population with identical natural frequencies. For this limit, we were able to reduce the governing equations using the Ott-Antonsen ansatz to a finite set of equations. By further assuming certain symmetries allowing for chimera states, we reduced these equations and were able to study the emergence of chimera states in the phase plane. Saddle node and Hopf bifurcation curves were determined using perturbative techniques to a high level of accuracy, as well as homoclinic bifurcation curves by observation of phase portraits. We were able to determine the stability diagram for the reduced systems, which includes one chimera where the desynchronized 'zone' or 'core' is of narrow width (SDS), and two

wide chimerae ($DS\,D$). The two $DS\,D$ chimerae distinguish themselves in that the phase angle of the order parameter, ψ, remains close to zero (for the first near global coupling) or close to π (for the second near local coupling for large A). The $S\,DS$ and the first $DS\,D$ chimera are bistable chimera attractors.

The equations (2.13) and(2.14) that we have analyzed were obtained by reducing the governing equations (2.1) in two different steps. Firstly, we reduced the problem of infinite degrees of freedom to a finite set of ordinary differential equations (2.10); in other words, we have restricted the dynamics of the system to the manifold defined by the Poisson kernel (2.7). The question whether or not this manifold in fact is an attractive, i.e. inertial manifold, is subject of current research. For the case of non-identical oscillators, i.e. for heterogeneous frequency distributions, a mathematical proof that it is indeed an attracting manifold, is in the process of being verified [39]. Findings from studying a variety of systems [5, 9, 22, 27] support this claim. The case of identical frequencies, for which results very recently have been published, is a different matter. Two teams, Pikovsky and Rosenblum [41], and Marvel *et al.* [31], have shown independently that the dynamics of each population can be reduced exactly to a flow described by three variables plus constants of motion. Moreover, it appears that for identical frequencies, instead of a *single* inertial manifold, there is a whole one-parameter *family* of invariant manifolds. In this picture, the OA manifold is a member of this family. These manifolds cannot be attracting anymore, and instead they are neutrally stable with regards to perturbations in transverse direction to themselves (a perturbation like this would result in moving the dynamics into a neighboring manifold). While we are fully aware of these results, they were unavailable to us at the time this study was done. Secondly, we have restricted the dynamics of the reduced equations (2.10) to the chimera symmetries

SDS and *DSD*. These symmetry manifolds need not be stable perturbations in transverse direction.

We therefore checked in numerical simulations that the chimera states also appear in the unreduced system (2.1) and that they indeed are subject to true attractors in this system. We found that the sequence of bifurcation scenarios of saddle node, Hopf and homoclinic bifurcations indeed is reproduced in the full system and that - even though we simulated the case with only small populations - the bifurcations appear close to the predicted critical values. The homoclinic bifurcation makes an exception in the sense that it occurs already for small A; however, we have argued that for large limit cycles, the trajectory would get kicked off the attractor because of the nearby saddle and finite size fluctuations. In conclusion, all chimera states, with exception of the second *DSD* state, have indeed proved to be true attractors in the unreduced system.

2.6.1 The Case of Heterogeneous Frequency Distributions

A recent study by Laing [22] generalizes the problem of a network with two oscillator populations investigated by [1] to the case of heterogeneous frequencies. Laing showed that for this and various other network topologies, the chimera state is robust –within limits– to heterogeneity in the intrinsic frequencies of the oscillators. In particular, he finds that the chimera state remains stable for populations with nearly identical oscillators, that is, with a narrow width of the distribution. The limit of letting the width of frequencies go to zero is well-defined and one retrieves the equations (2.10). The bifurcation diagrams obtained from our analysis should thus be the same as the one obtained for the dynamics of

oscillators with almost identical frequencies.

2.6.2 Aperiodicity and Chaos

In our setting of the problem with identical oscillators, we were able to find many solutions of the governing equations (2.1) that do not lie on the OA-manifold. Such states may be related to the quasiperiodic states shown to exist by Pikovsky *et al.* [41], and possibly also to chaotic states. The potential onset of chaos may be understood in the context that the dynamics of each population can be described by three variables [41, 31].

It is indeed not hard to find other attractors that do not belong to the OA-manifold. This may be demonstrated by starting the simulation with initial conditions that are off the OA-manifold, such as the Gaussian 'bumps' mentioned in Section 2.5, or by addition of noise to these initial conditions. We haven't gone much further in these questions, but have noticed irregular behavior in few of our simulations that may be aperiodic or chaotic. We think it may be possible to find something like a chaotic chimera state, and that more research should be done in this direction.

2.6.3 All-in-phase States

We have furthermore looked at two in-phase states that appear in our reduced equations, and analyzed their stability within the five dimensional equations given by (2.10) without assuming special symmetries. In the case where all populations are fully synchronized, i.e. $\rho_\sigma = 1$, the dynamics of the system

effectively becomes the one governed by three coupled oscillators. This case has already been studied in the context of three coupled sinusoidal limit cycle oscillators by Mendelowitz *et al.* [32] and for relaxation limit cycle oscillators by Bridge *et al.* [7], who found that two rotating waves, clockwise and counter-clockwise rotation, are possible.

2.6.4 Connection to the Ring of Oscillators and the Network with Two Oscillator Populations

It is important to mention the connection of our study with the work done by Abrams et al. [1], who studied a similar system with only two populations. With its two in-phase-locked populations, it is unclear whether the SDS or the DSD state compares best to their - using our terminology - SD chimera. Certainly, it can be said they both act like a two population system in disguise. In this sense, the two population system is a degenerate case of our triangular network.

The same authors also studied a continuum of oscillators on a ring [2, 3]. In our terms of oscillator populations, this system would be approximated by an infinite set of populations that are arranged in a ring structure. For the continuous ring, only a single chimera is known. Both SDS and DSD chimerae effectively act like a system made of two populations, but differ from one another, because the 'width' of drifting populations are different. In the case of the ring, the width of drifting oscillators is slightly larger than the synchronized region; from this point of view, the DSD chimera seems to be a closer relative than SDS.

An open question is: how is the behavior of discrete ring-like systems affected as we increase the number of populations until we reach the continuous case of the ring? One could for instance imagine that more and more chimera states get added as we increase the number of populations, and that they might be competing multistable attractors with respect to one another. But what happens as we take this continuum limit? Do they disappear, collapse or is it the case that only one of them, specifically, the one discussed in [3], wins the competition, dominates over all others and remains stable? We have confirmed that the SDS and the first DSD chimera are truly stable attractors in the unreduced system; it seems we can therefore not obtain any answers to this question from this study.

2.7 Acknowledgments

This research was supported in part by NSF Grant No. DMS-0412757 and CCF 0835706.

APPENDIX

Stability of Symmetric States

Existence of Symmetric States SSS

The states we consider here are fully synchronized, i.e. $\rho_\sigma = 1$ for all $\sigma = 1, 2, 3$. We have already explained in section II.B that $\rho_1 = \rho_3$ also implies $\phi_1 = \phi_3$. In order to derive a fixed point condition for these states, it is therefore sufficient to consider the equations that are already specialized to the symmetries SDS and DSD given by Equations (2.13) and (2.14). Applying the fixed point equation to either of them yields the condition

$$0 = (1 - A)(\cos\beta - \cos\beta\cos\psi + 3\sin\psi\sin\beta), \tag{2.28}$$

which is reduced to these cases:

$$A = 1, \tag{2.29}$$

$$\beta = 0 \quad \text{with } \cos\psi = 1,\ \sin\psi \neq 0, \tag{2.30}$$

$$\psi = 0, \tag{2.31}$$

$$\cos\beta = \frac{3\sin\beta\sin\psi}{\cos\psi - 1} \text{ with } \cos\psi \neq 1. \tag{2.32}$$

The first two conditions are the degenerate cases representing the A and β axis. The third condition corresponds to the fixed point $(\rho, \psi) = (1, 0)$, and the last to the position of the node that is constrained to move on the unit circle in the phase portraits, see Figs. 2.2 and 2.5.

Stability of SSS States

The computation of stability of these points is accomplished by computation of the Jacobian of the six dimensional system (2.10), with the coordinate system $(\rho_1, \rho_2, \rho_3, \phi_1, \phi_2, \phi_3)$, using a computer algebra system. Applying our symmetry assumptions, we find the eigenvalues

$$\lambda_k = \begin{pmatrix} 0 \\ -\sin\beta + 2(A-1)\sin(\beta+\psi) \\ (A-2)\sin\beta + (A-1)\sin(\beta-\psi) \\ (A-2)\sin\beta + (A-1)\sin(\beta-\psi) \\ (A-1)(2\sin\beta + \sin(\beta-\psi)) \\ (A-1)(3\cos\psi\sin\beta + \cos\beta\sin\psi) \end{pmatrix}. \tag{2.33}$$

The first eigenvalue is a manifestation of the rotational invariance of the system (the system only depends on phase differences and is effectively five dimensional).

We first compute the stability of the trivially symmetric state defined by $\psi = 0$. This highly degenerate state has the eigenvalues

$$\lambda_k = \sin\beta \begin{pmatrix} 0 \\ 2A-3 \\ 2A-3 \\ 2A-3 \\ 3(A-1) \\ 3(A-1) \end{pmatrix}. \tag{2.34}$$

As we only consider parameter values $A \in (0,1)$, this state is linearly stable only if $\beta \in (0, \pi)$.

The less trivial state with $\psi \neq 0$ must be considered in combination with the fixed point condition (2.32). The signs of these eigenvalues were not obtained analytically but rather by graphing the maximal eigenvalue in the (β, A)-plane. It turns out that this state has at least one positive eigenvalue except for the degenerate case where $\beta = 0, \pi$, and is thus always a saddle. This result is consistent with the behavior observed by inspection of the phase portraits of Eqs. (2.13) and (2.14) (in the case of SDS symmetry, the nontrivially symmetric state changes stability at $\beta = \pi$, but this holds only within the SDS-symmetry manifold, and has nothing to do with stability in the six (or five, for that matter) dimensional space.).

It is possible to obtain a similar stability result for the general case of a network with arbitrarily many populations N, for the trivially symmetric point satisfying $\rho_\sigma = 1$ and $\phi_1 = \phi_2 = ... = \phi_N$, using Gershgorin's circle theorem. In this general setting, the point also becomes linearly unstable as $\beta > \pi$ (provided that all row sums of the coupling matrix are strictly positive). Unfortunately, no similar result was obtained for the remaining $N - 2$ fixed points that may occur on the unit-sphere related to the general problem. The calculation is tedious and not represented here.

CHAPTER 3

CHIMERAE IN A NETWORK OF THREE OSCILLATOR POPULATIONS WITH VARYING NETWORK TOPOLOGY

3.1 Abstract

We study a network of three populations of coupled phase oscillators with identical frequencies. The populations interact nonlocally, in the sense that all oscillators are coupled to one another, but more weakly to those in neighboring populations than to those in their own population. Using this system as a model system, we discuss the influence of network topology on the existence of so called chimera states for the first time. In this context, the network with three populations represents an interesting case because the populations may either be connected as a triangle, or as a chain, thereby representing the simplest discrete network of either a ring or a line segment of oscillator populations. We introduce a special parameter that allows us to study the effect of breaking the triangular network structure, and to vary the network symmetry continuously such that it becomes more and more chain-like. By showing that chimera states only exist for a bounded set of parameter values we demonstrate that their existence depends strongly on the underlying network structures. We conclude that chimerae exist on networks with a chain-like character, which indicates that it might be possible to observe chimerae on a continuous line segment of oscillators.

3.2 Introduction

While studying a continuum of identical oscillators on a ring with nonlocal coupling, Kuramoto *et al.* [20] discovered a remarkable state where the population of oscillators splits into two subpopulations, where one is synchronized and the other is desynchronized, known as a *chimera state*. Since then several groups

have explored the nonlinear dynamics of chimerae [20, 3, 2, 43, 15, 16, 1, 22, 36]. Their emergence on the ring was first analyzed by Abrams and Strogatz [3, 2], who found that chimera states were born through a saddle node bifurcation. The state exists in systems of various different network topologies; for instance, Shima and Kuramoto [43] showed that chimerae also exist on 2D lattices with free boundaries in the shape of spiral waves. Other authors have been studying its appearance on variations of the Kuramoto model such as systems with delayed coupling [36, 42].

While various aspects about the emergence of chimerae have been addressed, the question of how the underlying network structure affects their existence has not been addressed systematically. We make a first step in this direction by studying a network of three oscillator populations with nonlocal coupling. A network with three nodes may either be arranged as a triangle or as a chain, and therefore represents the simplest case of a discrete network with ring-like or line-like character, respectively; the network structure will be determined by the nature of the coupling, as we explain later. The case of the triangular network has already been discussed in [28] where the authors show that two stable chimera states can coexist. In this study, we shall introduce a new parameter that allows us to break the rotational invariance inherent to the triangle and to vary the network structure continuously such that it becomes more and more chain-like.

We consider the case of infinitely many oscillators. This case is often considered a valid approximation, and using a recently developed method by Ott and Antonsen [38, 39] enables us to reduce this infinitely dimensional problem to a set of a finite ordinary differential equations, as discussed in [28, 1].

The article is structured as follows. In Section II we provide the definition of the system under investigation and explain how we intend to vary the character of the network structure by introduction of a special parameter. We then state the equations resulting from applying the Ott-Antonsen method and consider special symmetries that allow for chimerae. The analysis of the chimera states and their bifurcation scenarios follows in Section 3.4, where we analyze how the chimera states cease to exist as we vary the network structure using the above mentioned parameter. Section 3.6 summarizes our findings.

3.3 Governing Equations

The governing equations are given by

$$\frac{d}{dt}\theta_i^\sigma = \omega + \sum_{\sigma'=1}^{3} \frac{K_{\sigma\sigma'}}{N_{\sigma'}} \sum_{j=1}^{N_{\sigma'}} \sin(\theta_j^{\sigma'} - \theta_i^\sigma - \alpha), \tag{3.1}$$

where the phases of the oscillators are defined by θ; i denotes the individual oscillators belonging to the population with index $\sigma = 1, 2, 3$, each of which has N_σ oscillators; parameter α changes the character of the phases attraction.

The coupling kernel $K_{\sigma\sigma'}$ describes the strength between populations σ and σ'. The coupling strength is assumed to decay with increasing separation between the populations on the network. Within a population, the oscillators interact with strength $K_{\sigma\sigma'} = 1$. Neighboring populations couple more weakly, with strength $1 - A$ or $1 - cA$, as displayed in Fig. 3.1. We then have

$$K_{\sigma\sigma'} = \begin{pmatrix} 1 & 1-A & 1-cA \\ 1-A & 1 & 1-A \\ 1-cA & 1-A & 1 \end{pmatrix}. \tag{3.2}$$

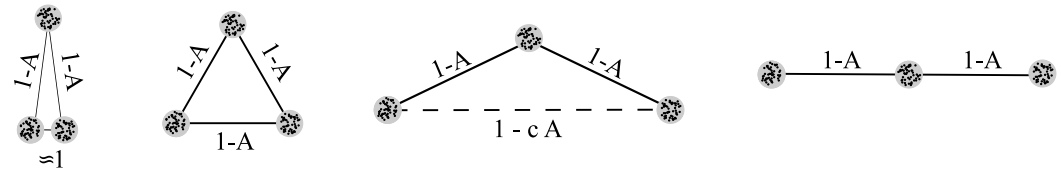

(i) c ≪ 1 (ii) c = 1 (iii) c > 1 (iv) c ≫ 1

Figure 3.1: Resulting network structures by varying parameter c. The gray disks symbolize populations, inhabited by individual oscillators symbolized by black dots. Their bidirectional coupling is represented by black lines. Each population has a self-coupling of unit strength 1. The population in what becomes the center for $c \neq 1$ is coupled to the neighboring populations with strength $1 - A$; the populations to the left and right are coupled with strength $1 - cA$. The case of a triangular network is obtained for $c = 1$; the character of the network has chain-like character for $c > 1$.

Thus, in the case of $A = 0$ we retrieve the case of a globally coupled network. Therefore, A may be thought of how 'far' we are away from global coupling. The introduction of parameter c in (3.2) generalizes our work in [28]: considering $c = 1$, we obtain the case of a triangular network with the same rotational symmetry as a continuum of oscillators on a ring, studied by [20, 3, 2]; for arbitrary c, it is a generalization of the problem with two populations discussed by Abrams *et al.* [1]. If we let $c \neq 1$ we break the rotational symmetry; in particular, for $c > 1$, the left and right populations interact less strongly with one another than they interact with what turns out to be the center population. Hence, parameter c implements the concept of increasing the distance between the outer left and right population, while their distance to the center remains constant: the network attains a chain-like character with $c > 1$. Our interest lies in positive coupling only and we therefore impose the constraints

$$c \cdot A \leq 1, \tag{3.3}$$

$$A \leq 1. \tag{3.4}$$

We have a strong interest in the case of coupling with $c > 1$ because of its close relation to line-like structures; but we shall relax this constraint during the subsequent analysis in favor of a deeper understanding of the bifurcation structure.

3.3.1 Reduced Equations and Symmetry Manifolds

In order to analyze the behavior of (3.1), we consider the limit of infinitely large populations, i.e. $N_\sigma \to \infty$. In this limit, one may describe the dynamics in terms of the oscillator density distribution $f^\sigma(\theta, t)$; furthermore, a complex order parameter is introduced, which describes the average of the oscillator phases:

$$z^\sigma(t) = \sum_{\sigma'=1}^{3} K_{\sigma\sigma'} \int_0^{2\pi} e^{i\theta'} f(\theta', t)\, d\theta'. \tag{3.5}$$

This entity represents the average for each population only rather than the sum over all of them, and is therefore referred to as a *local order parameter*. In this formulation of the problem, we are able reduce the problem to a finite set of equations, using an ansatz recently developed by Ott and Antonsen [38]. This method has been described in detail in [1, 28]; we omit the derivation here and simply state the reduced equations:

$$\begin{aligned} \dot{\rho}_\sigma &= \frac{1-\rho_\sigma^2}{2} \sum_{\sigma'=1}^{3} K_{\sigma\sigma'} \rho_{\sigma'} \sin(\phi_{\sigma'} - \phi_\sigma + \beta), \\ \dot{\phi}_\sigma &= \omega - \frac{1+\rho_\sigma^2}{2\rho_\sigma} \sum_{\sigma'=1}^{3} K_{\sigma\sigma'} \rho_{\sigma'} \cos(\phi_{\sigma'} - \phi_\sigma + \beta), \end{aligned} \tag{3.6}$$

where

$$\beta = \pi/2 - \alpha, \tag{3.7}$$

$$a_\sigma = \rho_\sigma e^{-i\phi_\sigma}, \tag{3.8}$$

$$\sigma \in \{1, 2, 3\} \tag{3.9}$$

and the density f is assumed to have the form

$$f^{\sigma} = \frac{1}{2\pi}\left\{1 + \left[\sum_{k=1}^{\infty}(a_{\sigma}(t)e^{i\theta})^{k} + c.c\right]\right\}. \tag{3.10}$$

These equations describe the dynamics of the oscillators in terms of two variables: ρ_{σ} is the modulus of the complex order parameter (3.5) describing the degree of synchronization for each population, whereas ϕ_{σ} is the angular order parameter representing the average phase of the oscillators in each population.

Before analyzing these equations, we shall focus our attention to specific symmetry manifolds. Perfectly synchronized populations have $\rho_{\sigma} = 1$ and desynchronized populations have $\rho_{\sigma} < 1$; the latter consists of oscillators that drift relative to one another and to the synchronized populations. Let S and D denote synchronized and desynchronized populations, respectively. In the triangular network, due to its rotational invariance, we could only distinguish two chimera states, namely SDS (sync-drift-sync) and DSD (drift-sync-drift). The situation is different here, and other chimerae are possible in the case of $c \neq 1$: SDD, SSD and their symmetry-equivalent reflections across the center population. These states are however not the focus of this study and are excluded in our analysis.

The SDS state is defined as $\rho_1 = \rho_3 = 1$ and $\rho \equiv \rho_2 < 1$, whereas the DSD state has $\rho \equiv \rho_1 = \rho_3 < 1$ and $\rho_2 = 1$. Because our coupling kernel (3.2) is symmetric, the symmetry $\rho_1 = \rho_3$ also implies $\phi_1 = \phi_3$; hence populations 1 and 3 are phase-locked (this still holds true for $c \neq 1$.). The phase difference of the angular order parameter between the synchronized and desynchronized states is defined by

$$\psi = \phi_1 - \phi_2 = \phi_3 - \phi_2. \tag{3.11}$$

Applying these symmetry assumptions to (3.6) and substituting the coupling

kernel defined in (3.2), we obtain the equations describing the SDS states

$$\begin{aligned}
\dot{\rho} &= \frac{1-\rho^2}{2}\left[2(1-A)\sin(\psi+\beta)+\rho\sin\beta\right], \\
\dot{\psi} &= -(2-cA)\cos\beta-(1-A)\rho\cos(-\psi+\beta) \\
&+ \frac{1+\rho^2}{2\rho}\left[2(1-A)\cos(\psi+\beta)+\rho\cos\beta\right],
\end{aligned} \tag{3.12}$$

and the DSD states

$$\begin{aligned}
\dot{\rho} &= \frac{1-\rho^2}{2}\left[(2-cA)\rho\sin\beta+(1-A)\sin(-\psi+\beta)\right], \\
\dot{\psi} &= -\frac{1+\rho^2}{2\rho}\left[(2-cA)\rho\cos\beta+(1-A)\cos(-\psi+\beta)\right] \\
&+ 2(1-A)\rho\cos(\psi+\beta)+\cos\beta.
\end{aligned} \tag{3.13}$$

Fixed points of (3.12) and (3.13) correspond to phase-locked solutions of the original system. The reduced equations (3.6) (after transformation into the corotating frame, i.e. $\phi_\sigma \rightarrow \phi_\sigma + \omega t$), and (3.12,3.13) share the property of being invariant under the following time-reversibility transformations:

$$(\beta, t, \psi) \rightarrow (-\beta, -t, -\psi), \tag{3.14}$$

$$(\beta, t) \rightarrow (\beta+\pi, -t). \tag{3.15}$$

Notice that the bifurcation structures that we study in the next section therefore repeat themselves in the (β, A)-plane accordingly.

In conclusion, we have reduced the governing equations (3.1) to a low dimensional system for the local order parameters, and we have cast our problem into a two dimensional system represented by Eqs. (3.12,3.13). This enables us to study the problem in the phase plane.

3.4 Bifurcation Behavior Near the Triangular Structure

We briefly summarize the findings for the triangular case $c = 1$ made in [28]; then we will study what happens to the bifurcation diagram as we break the symmetry. The associated bifurcation diagrams are shown in Fig. 3.2; the triangular case is shown in the left column and is compared to the symmetry breaking case in the right column. Now consider the case of SDS symmetry. We keep the parameter β fixed at $\beta = 0.05$ and increase the value of A step by step: close to global coupling, i.e. for small values of A, we only observe the in-phase SSS solution. For larger A further, a stable chimera is born in a saddle-node bifurcation. One step further, the chimera loses its stability through a Hopf bifurcation and a limit cycle is born, the state of which corresponds to a so-called *breathing chimera*. Increasing A even more, the limit cycle grows and eventually collides with the saddle and is destroyed in a homoclinic bifurcation. The saddle-node curve, Hopf and homoclinic bifurcation curves all intersect in the Bogdanov-Takens (BT) point of codimension two. The case of DSD symmetry exhibits a similar bifurcation structure: for small A, the same scenario as the one described for the SDS symmetry appears; but for larger A, the scenario is repeated in the upper part of the parameter plane in *reversed order* (with increasing values of A), as shown in Fig. 3.2. The bifurcation diagrams were obtained by inspection of phase portraits (points are shown as gray dots in the figure). Later we obtained the saddle node and Hopf curves in analytical form, by solving the fixed point equations (3.12,3.13) simultaneously with either the saddle node condition $\det(J) = 0$, or the Hopf condition $\mathrm{tr}(J) = 0$ with $\det(J) > 0$. The resulting equations may be solved using a series approach with β as a bifurcation parameter, as described previously in [28].

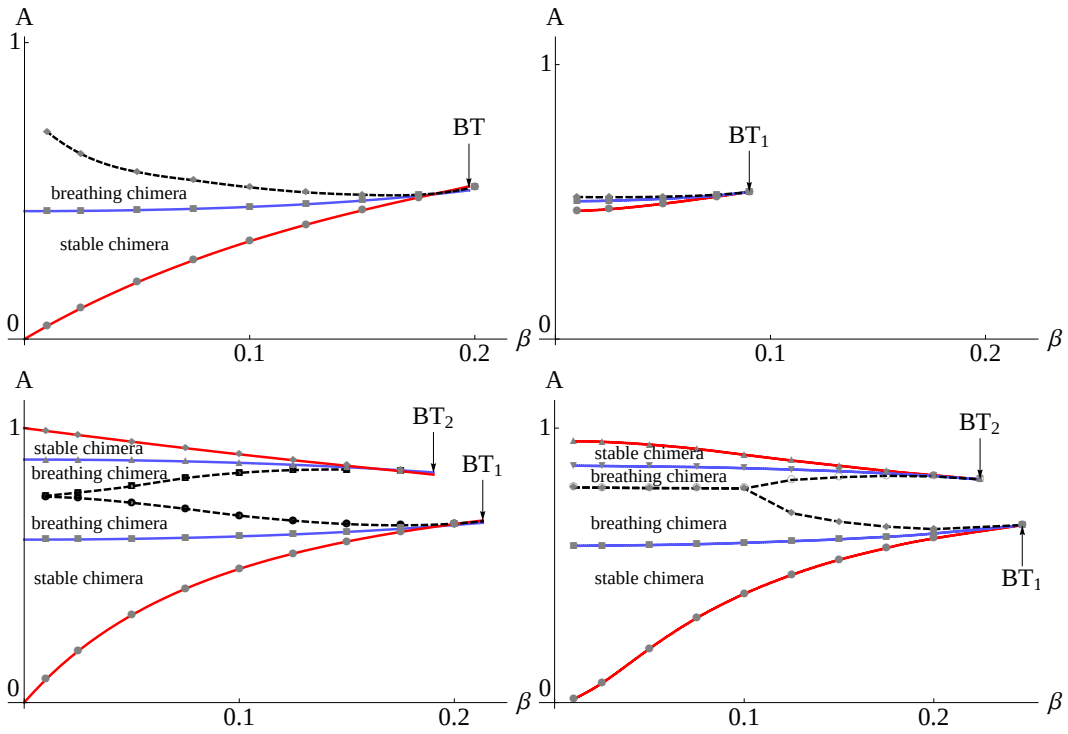

Figure 3.2: Effect of breaking the rotational symmetry on the bifurcation diagram for the SDS (top) and DSD (below) symmetry. The triangular case of ($c = 1$) is shown in the left, and $c = 1.1$ in the right row. The curves displayed are: the saddle-node curve (red), the Hopf curve (blue), and the homoclinic curve (black and dashed). Dots mark the bifurcation points obtained by inspection of the phase plane. The homoclinc curve is an interpolation based on these points, whereas the solid curves were obtained analytically.

We consider now the symmetry breaking case. The same perturbative method as described above is applicable for the case of $c \neq 1$ by letting c assume a desired value before computing the series coefficients. For brevity, we omit the listing of perturbation results for $A = A(\beta)$ for $c \neq 1$; no new insights emerge from this method [28] when we study $c \neq 1$. For sufficiently small values of $c > 1$, the bifurcation behavior is qualitatively similar to the triangular case. Results for $c = 1.1$ are shown in Fig. 3.2 in the right column: we ob-

serve a similar bifurcation scenario as before for the triangular case; but there is an important qualitative change: the region where parameter values allow for SDS chimerae (above) has shrunk in parameter space, whereas the attractor region of DSD chimerae (below) has grown. Remarkably, it looks as if the homoclinic curves for the DSD chimera coincide now for a range of small β values; unfortunately, we could not confirm this behavior analytically, as we were unable to determine the Melnikov integrals leading to homoclinic conditions. We consider this phenomenon as inessential for the matter of this study.

Moreover, the Bogdanov-Takens (BT) points have moved to the left and right, respectively, according to the shrinking or growing parameter regions of chimerae. We can check this by determining the locus of the BT points for $c = 1.1$. We solve the fixed point equations implied by Eqs. (3.12,3.13) together with the Hopf and saddle node conditions. Solving these equations numerically, we find the point for the SDS symmetry

$$(\beta, A)_{SDS} \approx (0.0902, 0.5361),$$

and the points for the DSD symmetry

$$(\beta, A)_{DSD,1} \approx (0.2467, 0.6466)$$
$$(\beta, A)_{DSD,2} \approx (0.2244, 0.8132),$$

indicated by arrows in Fig. 3.2. Comparing these numbers with our previous results from [28] confirms our observation.

3.5 Limits of Existence for Chimerae

We study now more generally what happens to the chimerae as we vary the values of c. Bifurcation diagrams for both chimera types were obtained by numerical continuation for a range of c values, displayed in Fig. 3.3. We have noted above that the attracting region for the SDS chimerae shrinks and the region for DSD chimerae grows when $c > 1$; conversely, as we consider the case $c < 1$, the opposite holds true. Just as before, the chimerae cease to exist completely at the point where the BT point touches the β-axis: this is where the saddle node, Hopf and homoclinic curves collapse.

We calculate the critical c values where this happens. The β-axis represents a singular limit and simply substituting $\beta = 0$ into the relevant equations defining the BT points, mentioned in the section before, leads nowhere; however we may obtain c_{crit} by using a perturbative approach. We use β as a perturbation parameter and consider the limit $\beta \to 0$. Inspecting the phase portrait of (3.12) we find that the SDS chimera is located near $\psi = 0$; therefore, the correct perturbation ansatz has to be

$$\psi = \psi_1 \beta + O(\beta^2). \tag{3.16}$$

Solving the resulting equations at first order of β, we find that the critical point for the SDS symmetry is located at

$$\begin{aligned} c_{crit} &= \frac{1}{12}\left(15 - \sqrt{33} + 2\sqrt{6\sqrt{33} - 30}\right) \approx 1.12356, \\ A_{crit} &= 1 - \frac{\sqrt{2}}{32}\left(\sqrt{33} - 1\right)^{3/2} \approx 0.54327, \\ \rho_{crit} &= \sqrt{\frac{\sqrt{33} - 1}{8}} \approx 0.770111. \end{aligned} \tag{3.17}$$

By the same token, for the DSD chimera associated with *small* values of A (lower

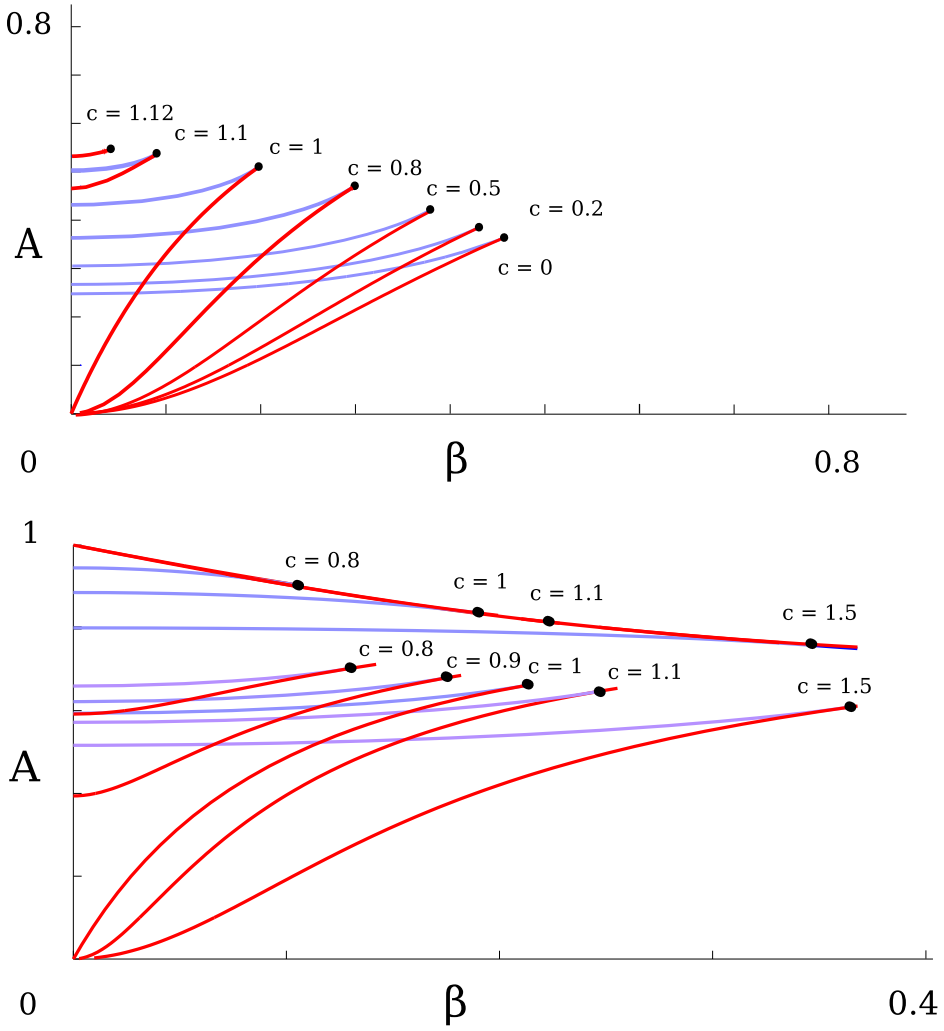

Figure 3.3: Bifurcation diagram for the SDS chimera (above) and the two DSD chimerae (below) in the (β, A)-plane for a range of c values. Saddle node (red) and Hopf curves (blue) are shown. The curves related to the SDS chimera collapse onto the β-axis at $c \approx 1.123$; conversely, the two DSD curves collapse on the axis at $c \approx 0.6778$ and $c = 2/3$, respectively. It is seen that the Bogdanov-Takens point (black dots) of the upper DSD chimera follows the associated saddle node curve as we vary c.

DSD chimera), we have

$$c_{crit} = \left(4774 - 350\sqrt{57} + \left(473\sqrt{7} - 53\sqrt{399}\right)\sqrt{(1+\sqrt{57}}\right)/3976 \approx 0.677869,$$

$$
\begin{aligned}
A_{crit} &= 1 + \sqrt{1 + \sqrt{57}}\left(11\sqrt{399} - 151\sqrt{7}\right)/1988 \approx 0.735569, \\
\rho_{crit} &= \frac{1}{2}\sqrt{\frac{1}{7}\left(1 + \sqrt{57}\right)} \approx 0.552586.
\end{aligned} \tag{3.18}
$$

Looking at Fig. 3.3, we notice that the saddle node curves coincide for all values of c; hence the associated set of BT points must also be located on this curve. Following the motion of the BT point as c decreases, we suspect that c becomes critical exactly when the BT point has reached $A = 1$. This looks like a limit of a higher order singularity than previously; indeed it is much harder to see in phase portraits at which angle ψ the BT point detaches from the β-axis. The correct perturbation ansatz turns out to be

$$
\psi = \frac{\pi}{2} + \psi_1 \beta + O(\beta^2). \tag{3.19}
$$

Solving again to first order in β results in

$$
\begin{aligned}
c_{crit} &= \frac{2}{3}, \\
A_{crit} &= 1, \\
\rho_{crit} &= \sqrt{\frac{1}{2}}.
\end{aligned} \tag{3.20}
$$

We conclude that SDS chimerae exist for parameter values $c \leq 1.12356$, and DSD chimera for $c \geq 0.677869$ and for $c \geq 2/3$, respectively (we shall see below that these limits for the existence of stable chimerae hold if $\beta > 0$).

Another interesting phenomenon is observed in Fig. 3.3: the saddle node curves of the SDS chimera pass through the origin $(\beta, A) = (0, 0)$ only if $c < 1$, but detach from the origin as soon as $c > 1$. The analogous behavior is seen for the DSD chimera, however for the converse case where $c < 1$. Thus having passed $c = 1$ and approaching c_{crit} implies the shrinking of the chimera attractor regions not only in the direction of the β-axis, but also along the direction of the

A-axis. To shed more light on this behavior, we calculate the locus of the saddle node transition $A = A(c)$ for $\beta \to 0$. These curves are this time simply obtainable by letting $\beta = 0$ while solving the saddle node condition together with the fixed point conditions. For SDS, we have:

$$A = \frac{3}{16c^3}\left(12c^2 - 9 \pm \sqrt{3}\sqrt{(3-2c)^3(1+2c)}\right), \tag{3.21}$$

$$A = 0, \tag{3.22}$$

and for DSD, we obtain the equations

$$\begin{aligned} 27(A-2)(A-1)^2A &= Ac\Big[-54 + 18A(6+c) + A^3c\left(18+c^2\right) \\ &\quad - 2A^2(27 + c(18+c))\Big], \end{aligned} \tag{3.23}$$

$$A = 1. \tag{3.24}$$

The resulting curves are shown in Fig. 3.4 (a) and (b). Recall that we are only interested in regions representing positive coupling, and regions where the coupling decays with increasing distance on the network graph. The second and forth quadrants in the (c, A)-plane represent regions where the coupling has a non-decaying character because of its entry with $(1 - cA) > 1$ in (3.2), and has therefore no line-like character. The entire lower half-plane has the same problem, but now due to the coupling kernel entry $(1 - A)$. In the quadrant that is left, we have to respect the constraints $A \leq 1$ and $1 \leq c \cdot A$; they are indicated by dotted lines. All these regions that are not of interest to us are shaded gray. The curves defined by (3.21)-(3.24) reach into these forbidden areas and are related to interesting dynamics; its nature is beyond the scope of this study and would require a more in-depth analysis.

Special points of interest are labeled in the diagrams: A is where the saddle node curve detaches from the β-axis, as shown in Fig. 3.3; the various B's

represent the critical points where the BT points, together with their stable and breathing chimera regimes, collide with the β-axis, for SDS and DSD symmetries; C denotes the point where the 'upper' DSD chimera boundary (3.24) intersects with the $1 = c \cdot A$ boundary; and finally, D denotes the analogous intersection with the $A = 1$ boundary.

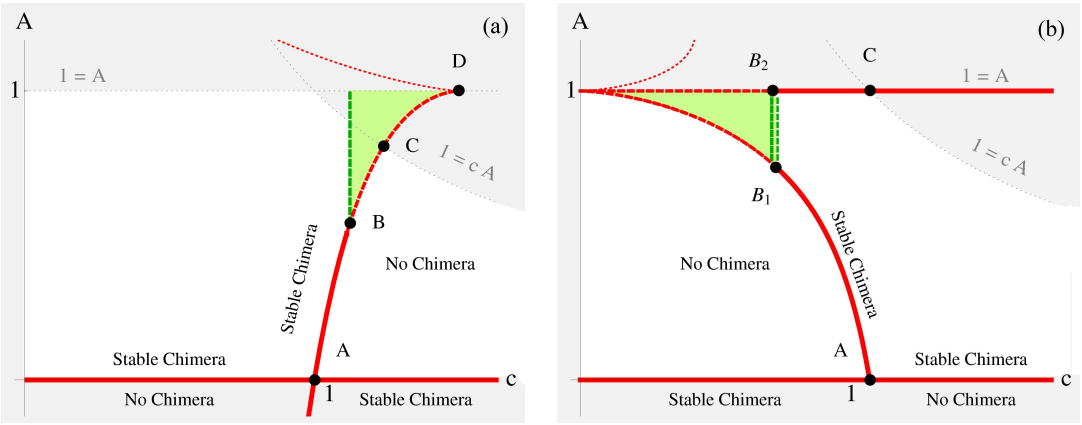

Figure 3.4: Boundaries for the occurrence of saddle node transitions in the (c, A)-plane (i.e. saddle node curves at $\beta = 0$), shown for the SDS symmetry (a) and DSD symmetry in (b). The gray dotted lines delineate the boundaries below which the coupling strength is positive. The black dots indicate points of special interest: **A**: $A = (1, 0)$ is where the saddle node curves detach from the origin (β, A)-plane. **B**: are the points for which the BT points collide with the β-axis leading to the annihilation of the chimera state; $B \approx (1.123, 0.543)$, $B_1 \approx (0.677, 0.735)$ and $B_2 = (2/3, 1)$. **C**: intersection with boundaries of positive coupling; $C_{SDS} = ((27 + \sqrt{27})/26, 26(27 + \sqrt{27}))$ and $C_{DSD} = (1, 1)$. **D**: intersection of the saddle-node boundary with $1 = A$; $D = (3/2, 1)$. The region where stable chimera only exist for $\beta < 0$ is shaded green.

Note that these curves do not delineate whole regions of stability: they represent the boundary of lowest possible A values where a saddle-node condition may occur (which by definition happens at least for the case of $\beta = 0$.). In other terms, chimerae that have been created through a saddle-node transition may

lose their stability through a Hopf and get destroyed in a homoclinic bifurcation for larger values of A. Areas where chimerae do not exist at all and regions with stable chimerae are labeled in Fig. 3.4.

The following applies for both SDS and DSD chimerae, but to keep things simple, let us only consider the case of the SDS symmetry. We have seen that below the curves defined by $\overline{OA}$ and $\overline{AB}$ chimerae do not exist; and that sufficiently close above these curves, there are stable chimerae. Now at point B, the BT point collides with the β-axis, and we expect not to see any chimerae beyond this point. But for $c > c_{crit}$, crossing the curve defined by $\overline{BD}$ we observe the creation of a saddle and a source with $\rho < 1$, corresponding to an *unstable* chimera. However, virtue to the symmetry in (3.14), $(\beta, \psi, t) \to (-\beta, -\psi, -t)$, a related stable node must exist for negative β. Hence, the green shaded region has chimerae that are stable for $\beta < 0$. If we extend our study to include $\beta < 0$, stable SDS chimerae in fact do also exist for $c > c_{crit}$, as well as two stable DSD chimera beyond their corresponding c_{crit}-values. We point out that however no Hopf or homoclinic bifurcations occur in the region beyond the critical point: these appear to be completely annihilated in point B where the BT points collide with the β-axis.

Similarly, the symmetry defined in (3.14) also affects the bifurcation structures (as displayed in Fig. 3.2) for the case before crossing c_{crit}: they are reflected across the β-axis, subject to the changes of stability, such that stable, but no breathing chimerae exist there too for $\beta < 0$.

3.6 Conclusion

We have investigated the problem of three nonlocally coupled oscillator populations, generalizing work done on networks with triangular symmetry [28]. We determined the limits (3.17), (3.18) and (3.20) for which stable chimera persist as the rotational invariance, inherent to the triangle, is broken. We found that these limits are valid for $\beta > 0$, but that stable chimera may exist otherwise beyond the critical c values. Thus chimera do indeed exist on chain-like topologies. It is therefore likely that chimerae may also exist for a continuum of oscillators on a line segment. Indeed, other studies of ours, not presented here, support this argument: we were able to find chimera states for such domains using a numerical iteration scheme based on Kuramoto's self-consistency equation as it is described in [20, 21]. In those simulations we used a kernel where the strength of coupling attenuates exponentially with distance.

By introducing parameter c, we were able to study the behavior of oscillator populations as we change the quality of the nonlocal coupling kernel (3.2); these changes are unrelated to the quality changes induced by parameter A, which controls how close we are to global coupling (or local coupling, for that matter). Conversely, parameter c controls the distance in between the 'left' and 'right' populations, and we may distinguish the different qualities it tunes into as visualized in Fig. 3.1: (i) for very small c, the left and right populations are very close, and see the center as a 'satellite' population. In this limit, there is only a SDS chimera. One could argue that it - though recall that its symmetry is broken - corresponds in our terminology to the SD chimera observed in two oscillator populations, reported in [1]; (ii) for $c = 1$, we retrieve the triangular case with rotational invariance; (iii) for $c > 1$ the network acts like a chain and

(iv) for very large c, the outer populations will almost only sense each other's motions indirectly via their coupling to the center population, as long as $1 \geq cA$, i.e. the coupling stays positive.

Note that the case $c \neq 1$ may indeed be looked at as a discretization of a line, even though we need c to be relatively close to 1 to observe stable chimera states. For instance, consider the case of a line-segment subject to a coupling kernel with exponential decay, as mentioned above; then we may tune the characteristic length scale of the kernel to match a desired value of c.

For future research, we suggest to investigate the continuum of oscillators on a line segment in more detail.

3.7 Acknowledgments

This research was supported in part by NSF Grant No. DMS-0412757 and CCF 0835706.

BIBLIOGRAPHY

[1] D. M. Abrams, R. E. Mirollo, S. H. Strogatz, and D. A. Wiley. Solvable model for chimera states of coupled oscillators. *Phys. Rev. Lett.*, 101:084103, 2008.

[2] D. M. Abrams and S. H. Strogatz. Chimera states for coupled oscillators. *Phys. Rev. Lett.*, 93:174102–174102, 2004.

[3] D. M. Abrams and S. H. Strogatz. Chimera states in a ring of nonlocally coupled oscillators. *Intern. Journ. Bif. Chaos*, 16(1):21–37, 2004.

[4] J. A. Acebrón, L. L. Bonilla, C. J. Pérez Vicente, F. Ritort, and R. Spigler. The Kuramoto model: A simple paradigm for synchronization phenomena. *Rev. of Mod. Physics*, 77(1):137–185, 2005.

[5] E. Barreto, B. Hunt, E. Ott, and P. So. Synchronization in networks of networks: The onset of coherent collective behavior in systems of interacting populations of heterogeneous oscillators. *Phys. Rev. E*, 77(3):36107, 2008.

[6] D. Battogtokh and Y. Kuramoto. Turbulence of nonlocally coupled oscillators in the Benjamin-Feir stable regime. *Phys. Rev. E*, 61(3):3227–3229, 2000.

[7] J. Bridge, L. Mendelowitz, R. Rand, S. Sah, and A. Verdugo. Dynamics of a ring of three coupled relaxation oscillators. *Communications in Nonlinear Science and Numerical Simulation*, 14(4):1598–1608, 2009.

[8] M. A. Buice and C. C. Chow. Correlations, fluctuations, and stability of a finite-size network of coupled oscillators. *Phys. Rev. E*, 76:031118, 2007.

[9] L. M. Childs and S. H. Strogatz. Stability diagram for the forced kuramoto model. *Chaos*, 18(043128), 2008.

[10] J. D. Crawford. Amplitude expansions for instabilities in populations of globally-coupled oscillators. *Journ. Stat. Physics*, 74(5):1047–1084, 1994.

[11] C. J. Goebel. Comment on "Constants of motion for superconductor arrays". *Physica D*, 80:18–20, 1995.

[12] D. Golomb, D. Hansel, B. Shraiman, and H. Sompolinsky. Clustering in globally coupled phase oscillators. *Phys. Rev. A*, 45(6):3516–3530, 1992.

[13] J. Guckenheimer and P. Holmes. *Nonlinear Oscillations, Dynamical Systems, and Bifurcations of Vector Fields, Springer-Verlag*. Springer New York, 1986.

[14] E. J. Hildebrand, M. A. Buice, and C. C. Chow. Kinetic theory of coupled oscillators. *Phys. Rev. Lett.*, 98(5):54101, 2007.

[15] Y. Kawamura. Chimera Ising walls in forced nonlocally coupled oscillators. *Phys. Rev. E*, 75:056204, 2007.

[16] Y. Kawamura and Y. Kuramoto. Hole structures in nonlocally coupled noisy phase oscillators. *Phys. Rev. E*, 76:047201, 2007.

[17] I. Z. Kiss, W. Wang, and J. L. Hudson. Populations of coupled electrochemical oscillators. *Chaos*, 12(252), 2002.

[18] Y. Kuramoto. International symposium on mathematical problems in theoretical physics. *Lecture Notes in Physics*, 39, 1975.

[19] Y. Kuramoto. *Chemical Oscillators, Waves and Turbulence*. Springer, Berlin, 1984.

[20] Y. Kuramoto and D. Battogtokh. Coexistence of coherence and incoherence in nonlocally coupled phase oscillators. *Nonlin. Phen. Complex Systems*, 5(4):380–385, 2002.

[21] Y. Kuramoto, S. Shima, D. Battogtokh, and Y. Shiogai. Mean-field theory revives in self-oscillatory fields with non-local coupling. *Progr. of Theor. Physics*, 161:127, 2006.

[22] C. R. Laing. Chimera states in heterogeneous networks. *Chaos: An Interdisciplinary Journal of Nonlinear Science*, 19:013113, 2009.

[23] C. R. Laing and C. C. Chow. Stationary bumps in networks of spiking neurons. *Neural Computation*, 13(7):1473–1494, 2001.

[24] C. R. Laing and A. Longtin. Noise-induced stabilization of bumps in systems with long-range spatial coupling. *Physica D: Nonlinear Phenomena*, 160(3-4):149–172, 2001.

[25] S. D. Makovetskiy and D. N. Makovetskii. *arXiv preprint*, 0805(1319v1), 2005.

[26] S. D. Makovetskiy and D. N. Makovetskii. Emergence, competition and dynamical stabilization of dissipative rotating spiral waves in an excitable medium: A computational model based on cellular automata. *arXiv preprint nlin.CG*, (0805.1319), 2008.

[27] E. A. Martens, E. Barreto, S. H. Strogatz, E. Ott, P. So, and T. M. Antonsen. Exact results for the Kuramoto model with a bimodal frequency distribution. *Phys Rev E*, 79:026204, 2009.

[28] E. A. Martens and S. H. Strogatz. Bistable chimerae on a triangular network of oscillator populations. *arXiv preprint nlin.PS*, 2009.

[29] E. A. Martens and S. H. Strogatz. Chimerae in a network of three oscillator populations with varying network topology. *arXiv preprint nlin.PS*, 2009.

[30] E. A. Martens and S. H. Strogatz. A solvable model for chimera states in spiral waves. *(in preparation)*, 2009.

[31] S. A. Marvel and S. H. Strogatz. Invariant submanifold for series arrays of Josephson junctions. *Chaos*, 19:013132, 2009.

[32] L. Mendelowitz, A. Verdugo, and R. Rand. Dynamics of three coupled limit cycle oscillators with application to artificial intelligence. *Communications in Nonlinear Science and Numerical Simulation*, 14(1), 2009.

[33] A. S. Mikhailov, S. H. Zanette, Y. M. Zhai, I. Z. Kiss, and J. L. Hudson. Cooperative action of coherent groups in broadly heterogeneous populations of interacting chemical oscillators. *Proc. Natl. Acad. Sci USA*, 101:10890, 2004.

[34] R. E. Mirollo, S. A. Marvel, and S. H. Strogatz. Sinusoidally coupled phase oscillators evolve by Mobius group action. *arXiv*, 0904.1680v1, 2009.

[35] E. Montbrió, J. Kurths, and B. Blasius. Synchronization of two interacting populations of oscillators. *Phys. Rev. E*, 70(5):56125, 2004.

[36] O. E. Omel'chenko, Y. L. Maistrenko, and P. A. Tass. Chimera states: The natural link between coherence and incoherence. *Phys. Rev. Lett.*, 100:044105, 2008.

[37] E. Ott. *Chaos in Dynamical Systems*. Cambridge University Press, 2002.

[38] E. Ott and T. M. Antonsen. Low dimensional behavior of large systems of globally coupled oscillators. *Chaos*, 18:037113, 2008.

[39] E. Ott and T. M. Antonsen. Long time evolution of phase oscillator systems. *Arxiv preprint arXiv:0902.2773*, 2009.

[40] E. Ott, J. H. Platig, T. M. Antonsen, and M. Girvan. Echo phenomena in large systems of coupled oscillators. *Chaos*, 18:037115, 2008.

[41] A. Pikovsky and M. Rosenblum. Partially integrable dynamics of hierarchical populations of coupled oscillators. *Phys. Rev. Lett.*, 101:264103, 2008.

[42] G.C. Sethia, A. Sen, and F.M. Atay. Clustered chimera states in delay-coupled oscillator systems. *Phys. Rev. Lett.*, 100:144102, 2008.

[43] S. Shima and Y. Kuramoto. Rotating spiral waves with phase-randomized core in nonlocally coupled oscillators. *Phys. Rev. E*, 69:036213, 2004.

[44] S. H. Strogatz. From Kuramoto to Crawford: exploring the onset of synchronization in populations of coupled oscillators. *Physica D: Nonlinear Phenomena*, 143(1-4):1–20, 2000.

[45] S. H. Strogatz, R. E. Mirollo, and P. C. Matthews. Coupled nonlinear oscillators below the synchronization threshold: Relaxation by generalized Landau damping. *Phys. Rev. Lett.*, 68(18):2730–2733, 1992.

[46] John J. Tyson. Introduction to bifurcation theory. http://mpf.biol.vt.edu/research/generic_model/main/pp/intro.php.

[47] S. Watanabe and S. H. Strogatz. Constants of motion for superconducting Josephson arrays. *Physica D*, 74(3-4):197–253, 1994.

[48] J. A. C. Weideman. Computation of the complex error function. *SIAM Journal on Numerical Analysis*, 31(5):1497–1518, 1994.

[49] K. Wiesenfeld and J. W. Swift. Averaged equations for Josephson junction series arrays. *Phys. Rev. E*, 51, 1995.

[50] S. Yamaguchi. Synchronization of cellular clocks in the suprachiasmatic nucleus. *Science*, 302:1408–1412, 2003.